Early-wave macrophages control late hematopoiesis

Sara Monticelli, Alina Sommer, Zeinab Alhajj Hassan, Clarisabel Garcia Rodriguez, Kémy Adé, Pierre Cattenoz, Claude Delaporte, Elisa Gomez Perdiguero, Angela Giangrande

Article

Developmental Cell

Early-wave macrophages control late hematopoiesis

Graphical abstract

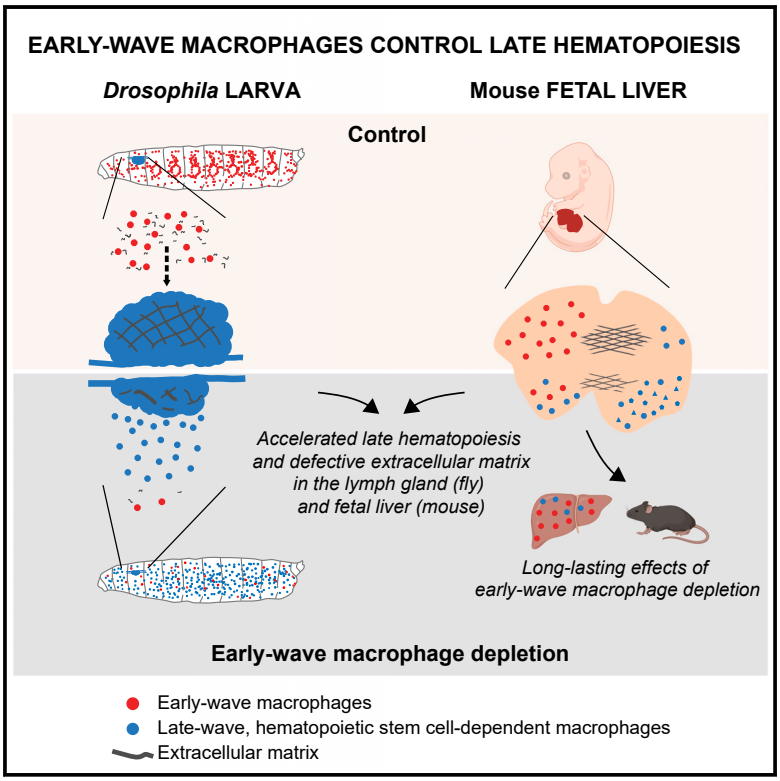

Highlights

- Macrophages remodel the developing hematopoietic environment throughout evolution
- Early-wave macrophage depletion accelerates late, stem-cell-dependent hematopoiesis
- Early-wave-derived extracellular matrix molecules control the fly late hematopoiesis
- Early-wave macrophage depletion has long-lasting effects on hematopoiesis

Authors

Sara Monticelli, Alina Sommer, Zeinab AlHajj Hassan, ..., Claude Delaporte, Elisa Gomez Perdiguero, Angela Giangrande

Correspondence

elisa.gomez-perdiguero@pasteur.fr (E.G.P.), angela@igbmc.fr (A.G.)

In brief

Monticelli et al. investigate the interaction between hematopoietic waves during development. Depletion of early-wave macrophages accelerates late, stem-cell-dependent hematopoiesis in flies and mice, which relies on extracellular matrix molecules derived from early-wave macrophages.

Monticelli et al., 2024, Developmental Cell *59*, 1284–1301
May 20, 2024
https://doi.org/10.1016/j.devcel.2024.03.013

CellPress

CellPress

Developmental Cell

Article

Early-wave macrophages control late hematopoiesis

Sara Monticelli,[1,2,3,4] Alina Sommer,[5,6] Zeinab AlHajj Hassan,[1,2,3,4] Clarisabel Garcia Rodriguez,[5,6] Kémy Adé,[5] Pierre Cattenoz,[1,2,3,4] Claude Delaporte,[1,2,3,4] Elisa Gomez Perdiguero,[5,7,*] and Angela Giangrande[1,2,3,4,7,8,*]

[1]IGBMC, Institut de Génétique et de Biologie Moléculaire et Cellulaire, 67400 Illkirch, France
[2]Centre National de la Recherche Scientifique, UMR 7104, 67400 Illkirch, France
[3]Institut National de la Santé et de la Recherche Médicale, UMR, S 1258, 67400 Illkirch, France
[4]Université de Strasbourg, IGBMC UMR 7104- UMR-S 1258, 67400 Illkirch, France
[5]Macrophages and endothelial cells unit, Department of Developmental and Stem Cell Biology, Institut Pasteur, Université Paris Cité, UMR3738 CNRS, 75015 Paris, France
[6]Sorbonne Université, Collège doctoral, 75005 Paris, France
[7]These authors contributed equally
[8]Lead contact
*Correspondence: elisa.gomez-perdiguero@pasteur.fr (E.G.P.), angela@igbmc.fr (A.G.)
https://doi.org/10.1016/j.devcel.2024.03.013

SUMMARY

Macrophages constitute the first defense line against the non-self, but their ability to remodel their environment in organ development/homeostasis is starting to be appreciated. Early-wave macrophages (EMs), produced from hematopoietic stem cell (HSC)-independent progenitors, seed the mammalian fetal liver niche wherein HSCs expand and differentiate. The involvement of niche defects in myeloid malignancies led us to identify the cues controlling HSCs. In *Drosophila*, HSC-independent EMs also colonize the larva when late hematopoiesis occurs. The evolutionarily conserved immune system allowed us to investigate whether/how EMs modulate late hematopoiesis in two models. We show that loss of EMs in *Drosophila* and mice accelerates late hematopoiesis, which does not correlate with inflammation and does not rely on macrophage phagocytic ability. Rather, EM-derived extracellular matrix components underlie late hematopoiesis acceleration. This demonstrates a developmental role for EMs.

INTRODUCTION

The immune system of adult vertebrates is sustained throughout life by a classical differentiation cascade from hematopoietic stem cells (HSCs), which are maintained and regulated through interactions with their micro-environment or niche. As the pool of HSCs is established during development, with no *de novo* generation during adulthood, embryonic perturbations can affect the development of HSCs, thereby leading to long-lasting changes in the capacity of organisms to respond later on to (immune) challenges. It is thus crucial to understand the cellular and molecular events regulating HSC homeostasis during development, and here, we focused on the function of macrophages in this process. Indeed, before the emergence of HSCs, macrophages produced by earlier (HSC-independent) progenitor waves colonize the embryo and participate to key physiological processes such as metabolism; development; and tissue remodeling by phagocytosing debris/apoptotic cells and by secreting a wide range of molecules, including extracellular matrix (ECM) components/-modifying enzymes, growth factors, and cytokines.[1] They are very abundant in the fetal hematopoietic niche where HSCs expand and differentiate and are thus ideal candidates to modulate HSC micro-environment. The establishment of the immune system by successive waves is evolutionarily conserved. We combined the advantages of two model organisms, the invertebrate *Drosophila melanogaster* and the mammalian mouse model, for complementary and synergetic investigation of the contribution of early, HSC-independent macrophages to the establishment of the adult immune system.

Mouse hematopoiesis occurs in at least three distinct waves during embryogenesis, with macrophages being generated during each wave. Macrophages from the first two waves (primitive and erythro-myeloid progenitors (EMPs) emerging from the extra-embryonic yolk sac) migrate to the embryo proper and colonize, among other tissues, the nascent fetal liver (FL) starting at embryonic day (E) 9.[2–5] The third hematopoietic wave starts intra-embryonically at around E9.5, when embryonic multipotent progenitors (eMPPs) followed by HSCs emerge from the aorta-gonado-mesonephros region and major arteries[6,7] and migrate to the FL to expand and differentiate[8] (Figure 1A). Contrary to what was initially thought, fetal HSCs do not contribute to mature blood cell production until birth.[9–12] Before birth, HSCs migrate to the bone marrow niche, where they are maintained throughout adulthood and generate all blood cell types[13,14](Figure 1A). Throughout fetal life, macrophages are generated from yolk-sac-derived HSC-independent progenitors and are thus referred to as embryonic or early-wave macrophages (EMs). Murine HSCs thus expand in a FL already colonized by EMs, recently reported to be potentially involved in HSC emergence in mouse embryos.[15] However, whether mouse EMs modulate

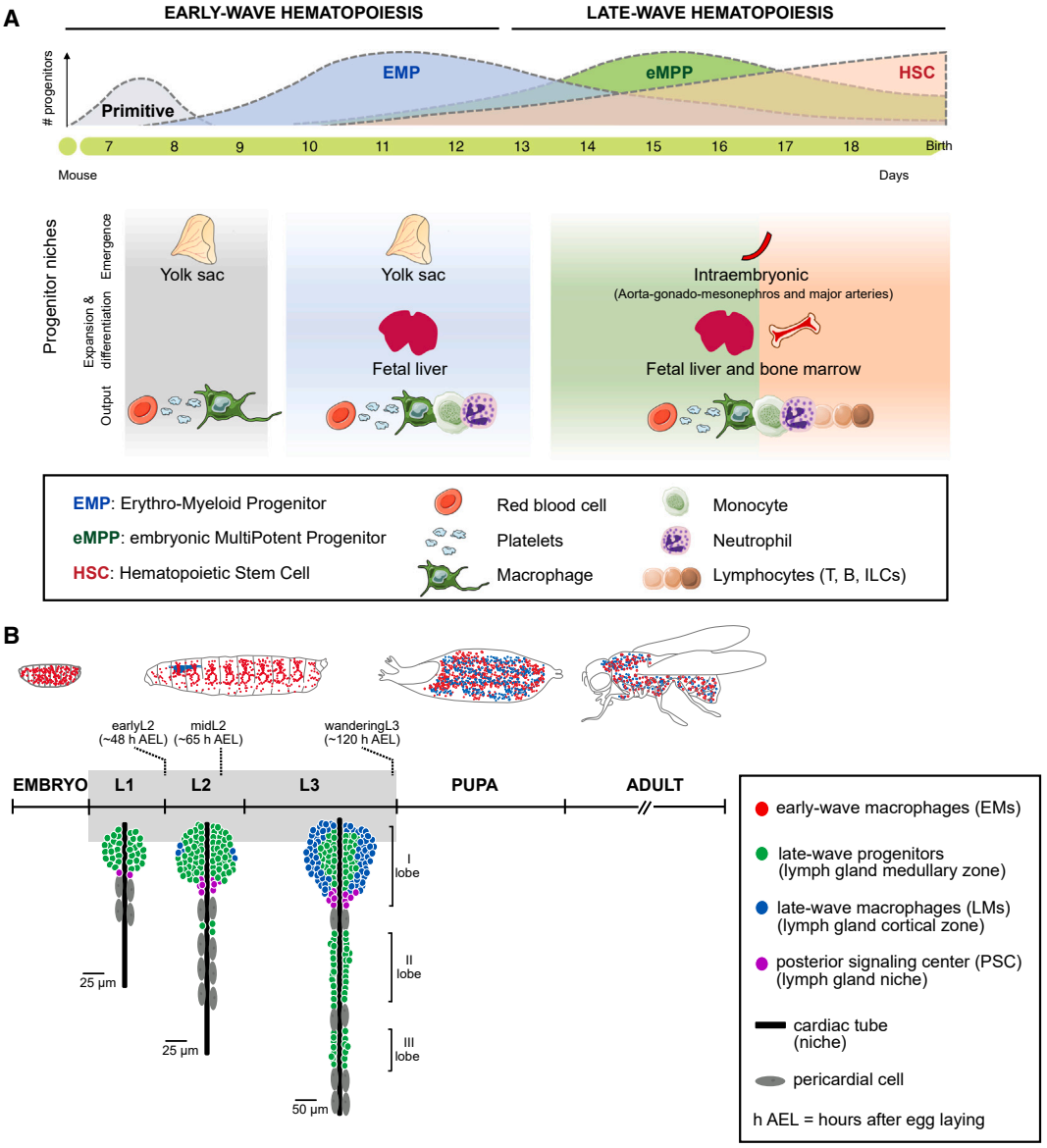

Figure 1. Mammalian and *Drosophila* hematopoiesis

Schematics representing early and late hematopoietic waves in (A) mammals and (B) *Drosophila*.

HSC-derived hematopoiesis after HSC emergence is currently unknown.

The immune system of *Drosophila* is simpler, with few cell types accounting for innate immunity only (generally called hemocytes). Under normal conditions, macrophages (also called plasmatocytes) comprise 90%–95% of *Drosophila* hemocytes, while crystal cells, platelet-like cells helping the wound healing process, account for 2%–5% of the hemocytes. For the sake of simplicity, we will refer to hemocytes as macrophages. *Drosophila* macrophages are produced during two distinct waves. Primitive or Ems differentiate from the procephalic mesoderm of the early embryo and colonize the whole organism. Late-wave macrophages (LMs) originate from a specialized hematopoietic organ, the lymph gland, which reaches maturation and releases LMs after the larval stages. LMs and Ems co-exist in the adult at a 1:2 ratio (for a recent review, see Banerjee et al.[16]) (Figure 1B). The progenitor cells of the lymph gland are considered as bona fide HSC-like cells, and their maintenance/differentiation relies on niche-derived cues that also regulate mammalian HSCs in the FL and bone marrow niches (e.g., Hh,[17,18] Dpp/BMP,[19,20] Wg/Wnt,[21,22] Slit/Robo,[23] and Col/Ebf[24,25] pathways). Whether EMs interact with the lymph gland and regulate late hematopoiesis is not known. Nevertheless, EMs are free to circulate in the hemolymph (analogous of the vertebrate blood), bathing all the organs of the *Drosophila* larva, including the developing lymph gland. Moreover, EMs impact the immune response mounted by the late hematopoietic wave,[26] calling for homeostatic interactions between the two waves.

Here, we show that EMs play a key role in modulating late hematopoiesis and that this role is evolutionarily conserved. The

depletion of *Drosophila* EMs accelerates the maturation of the lymph gland and LM differentiation. This phenotype does not rely on inflammation or on EMs' phagocytic function but rather on EM-derived ECM molecules ensuring proper architecture of the lymph gland. Similarly, EM depletion during mouse FL hematopoiesis triggers premature differentiation of HSCs not only into macrophages but also into monocytes and neutrophils in the FL, whose ECM is defective. Importantly, transient EM depletion *in utero* leads to long-lasting changes in adult HSCs, with increased myeloid potential at the expense of lymphoid-biased progenitors. Revealing the so far largely unexplored link between the hematopoietic waves opens important perspectives in basic and medical science, with the potential role of HSC-independent hematopoiesis in shaping the adult immune system, thus influencing the risk of developing diseases after birth.

RESULTS

Fly late hematopoiesis is affected by EM depletion

To assess how late hematopoiesis responds to the loss of EMs in *Drosophila*, we depleted the larva of macrophages and examined the state of the lymph gland.

The lymph gland is a paired organ sitting on the cardiac tube and consisting of lobes named from primary to tertiary (or more) by proceeding antero-posteriorly (Figure 1B). Primary lobes start differentiating at mid second larval instar (midL2), whereas the posterior lobes mature only at pupal stage, when the primary lobes undergo histolysis and release LMs.[27,28] Under normal conditions, the primary lobes are fully mature, yet still intact, at wandering third larval instar (wL3) and mainly consist of a cortical zone containing differentiated LMs; a medullary zone containing progenitors; and the posterior signaling center (PSC), the lymph gland signaling niche[16] (Figure 1B).

Previous works have shown that genetic macrophage depletion throughout larval development (from the first larval instar [L1] to wL3) triggers a severe loss of macrophages in wL3 larvae[29–33] and precocious rupture of the lymph gland primary lobes.[33] To deplete macrophages, we hence used a similar approach, upon expressing the cell death gene *head involution defective* (*UAS-hid*)[34] (together with that of the GFP, *UAS-GFP*) under the control of the macrophage-specific *Hemolectin* (*Hml*) Gal4 driver (*HmlΔGal4*) (Figures S1A–S1H). *HmlΔGal4* is active from L1 onward,[35,36] allowing postembryonic depletion of macrophages and preventing the embryonic lethality induced by earlier macrophage depletion.[30,37] We confirmed the histolysis of the primary lobes and showed that the lymph gland posterior lobes are oversized and show increased cell differentiation (Figures S1E–S1H). This approach, however, does not allow to disclose the contribution of EMs on lymph gland development because by midL2 *Hml* starts being expressed in differentiating LMs.[38,39] These cells are likely targeted by the depletion strategy and undergo apoptosis, leading to inflammation, as documented by the presence of activated immune cells, called lamellocytes and marked with Atilla[40] and L4,[41] in wL3 lymph gland and hemolymph (Figures S1H and S1I).[31,33]

To assess whether the specific loss of EMs affects late hematopoiesis, we depleted Hml$^+$ macrophages and analyzed midL2 larvae (∼65 h after egg laying [AEL]) (Figure 2A) before massive differentiation of Hml$^+$ LMs in the lymph gland (Figure 2G). Depleted larvae show no Hml$^+$ EMs (Figure 2B), and the number of EMs per larva is drastically reduced (∼25%, Figure 2C), with only few cells detected by immunolabeling (Figure 2D). This suggests that EM numbers could be overestimated by brightfield counting due to the presence of dying cells and cell debris that are washed out during the labeling protocol. Consistently, the hemolymph of depleted larvae shows labeling with the apoptotic marker cleaved caspase Dcp-1 (Dcp1)[42](Figure 2E). The few remaining cells are labeled by macrophage markers, such as Peroxidasin (Pxn) and Hemese (He)[33,43,44] and do not express *Hml* (Figures 2D and 2E). However, these cells do not resemble canonical macrophages, and quantitative reverse-transcription PCR (RT-qPCR) assays performed at the beginning of the second larval instar (earlyL2, ∼48 h AEL) reveal a poor expression of *Pxn* and of the phagocytic receptor encoding genes *eater* and *NimC1*[45,46] (Figure 2F). This suggests that the Pxn signal revealed by immunolabeling at midL2 likely results from a high stability of the protein, and the cells left after EM depletion lose macrophage marker expression and possibly phagocytic function, which is hardly assessable due to the scarce number of macrophages surviving the depletion.

We next analyzed the midL2 lymph gland, consisting mostly of the sole primary lobes[16] (Figures 1B and 2G). The volume of the lymph gland from depleted larvae is almost doubled, and the primary lobe cellularity is significantly higher than in controls (Figures 2G and 2H). Increased cell proliferation is detected by earlyL2 using the mitotic marker phosphorylated Ser10 of histone 3 (PH3)[47] but not by midL2 (Figures S2A–S2D),[39] suggesting earlyL2 as the phenocritic phase for the over-proliferation of the larval hematopoietic organ. This phenotype is unlikely to be caused by the expression of Hid in the few Hml$^+$ LMs normally present in the earlyL2 lymph gland (14.75 ± 3.46 Hml$^+$ cells out of 450 ± 28 DAPI$^+$ nuclei; mean ± standard error) (Figure 3C). Moreover, several Hml$^+$ and/or Pxn$^+$ LMs are present in the midL2 lymph gland upon EM depletion, and they spread throughout the primary lobes (Figure 2G), indicating a premature differentiation that overrides the proper patterning of the lymph gland (Figure 1B).

Extensive cell death occurs in the midL2 lymph gland of depleted animals (Figure 2I). This phenotype may have different origins. The premature appearance of Hml$^+$ macrophages in the lymph gland could induce *hid* expression in LMs. Dying LMs could also trigger apoptosis in neighboring cells in a non-cell-autonomous manner.[48] Precocious and strong differentiation of the organ could also indirectly lead to apoptotic events. In line with these non-mutually exclusive hypotheses, we detect Dcp1 expression in Hml$^+$ and Hml$^-$ macrophages, some of which are close to dying Hml$^+$ macrophages (Figure 2I). Finally, several lamellocytes are detected in the lymph gland of depleted larvae (Figure 2J), indicating an inflammatory state likely resulting from the widespread apoptosis.[31]

Overall, these experiments reveal that depleting EMs leads to overgrowth and premature differentiation of the late hematopoiesis organ, which also shows inflammatory phenotypes.

Fly EM depletion accelerates the physiological development of the lymph gland

To formally discriminate whether the observed precocious maturation of the lymph gland is due to inflammation-related

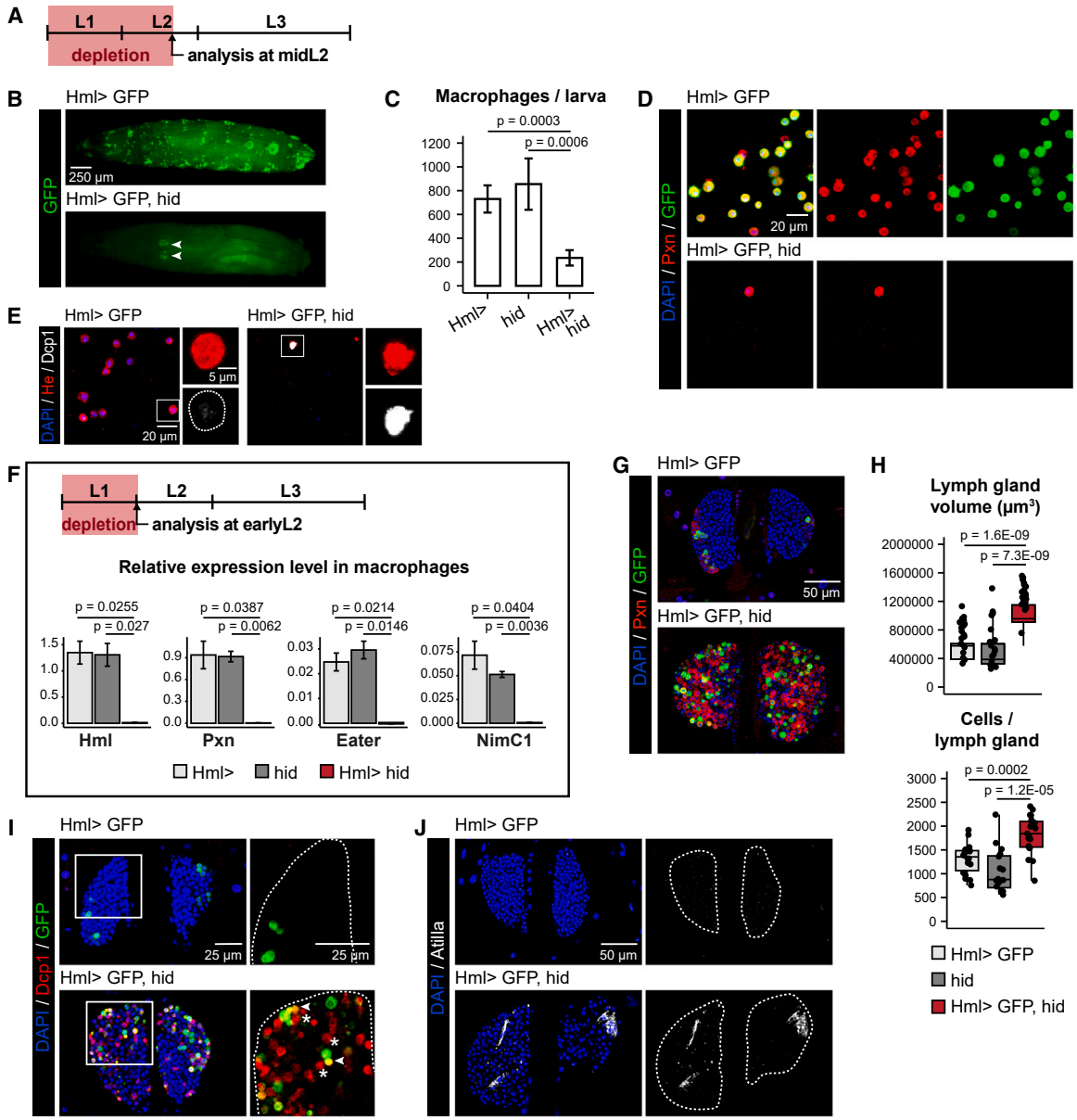

Figure 2. Fly late hematopoiesis is affected by early-wave macrophage (EM) depletion

(A) Experimental setup adopted in (B)–(E) and (G)–(J). The *Hml⊿Gal4* driver was used to express the cell death gene *hid* in macrophages from the beginning of the larval life until mid-second larval instar (midL2) ~65 h after egg laying (AEL) with animals raised at 25°C. Only in (F), the depletion was carried out until early second larval instar (earlyL2) ~48 h AEL. Both settings ensure specific depletion of early-wave macrophages (EMs) in the larva. A reporter GFP was used to reveal *Hml* expression.

(B) Dorsal view of a control larva and an EM-depleted larva (anterior on the left, posterior on the right). Arrowheads point the lymph gland primary lobes.

(C) Number of macrophages per larva (mean ± standard deviation [SD]) assessed by brightfield counting (N ≥ 3).

(D and E) Immunolabeling of bled macrophages. (D) The anti-Pxn macrophage marker is in red, anti-GFP in green; **(E)** the anti-He macrophage marker is in red, the anti-Dcp1 apoptotic marker is in gray. Nuclei are labeled with DAPI in blue.

(F) Top: experimental setup. Bottom: relative expression level (mean ± standard error [SE]) of Hml, Pxn, Eater, and NimC1 assessed by RT-qPCR on macrophages bled from control or EM-depleted larvae (3 independent replicates).

(G) Lymph gland immunolabeling. Anti-Pxn is in red, and anti-GFP in green; nuclei are labeled with DAPI in blue. N ≥ 15.

(H) Lymph gland primary lobes' volume (top) and number of cells (bottom) (N ≥ 16).

(I and J) Lymph gland immunolabeling with (I) anti-Dcp1 in red, anti-GFP in green (J) the anti-Atilla lamellocyte marker in gray; nuclei are labeled with DAPI in blue. (I) White squares define the area shown in the insets as Dcp1 and GFP merge. Dashed lines indicate the perimeter of the lymph gland lobes, arrowheads point $Hml^{+}Dcp1^{+}$ macrophages, asterisks point $Hml^{-}Dcp1^{+}$ macrophages (N ≥ 8). Detailed genotypes: *w;HmlΔGal4,UAS-2XEGFP/+;+* (Hml > GFP), *w;UAS-hid/+;+* (hid), *w;HmlΔGal4,UAS-2XEGFP/UAS-hid;+* (Hml > GFP, hid), *w;HmlΔGal4/+;+* (Hml>), *w; HmlΔGal4/UAS-hid;+* (Hml > hid). Confocal images are shown as full-stack projections for bled macrophages and representative single sections for lymph glands unless otherwise specified. Statistics: two-tailed unpaired t test.

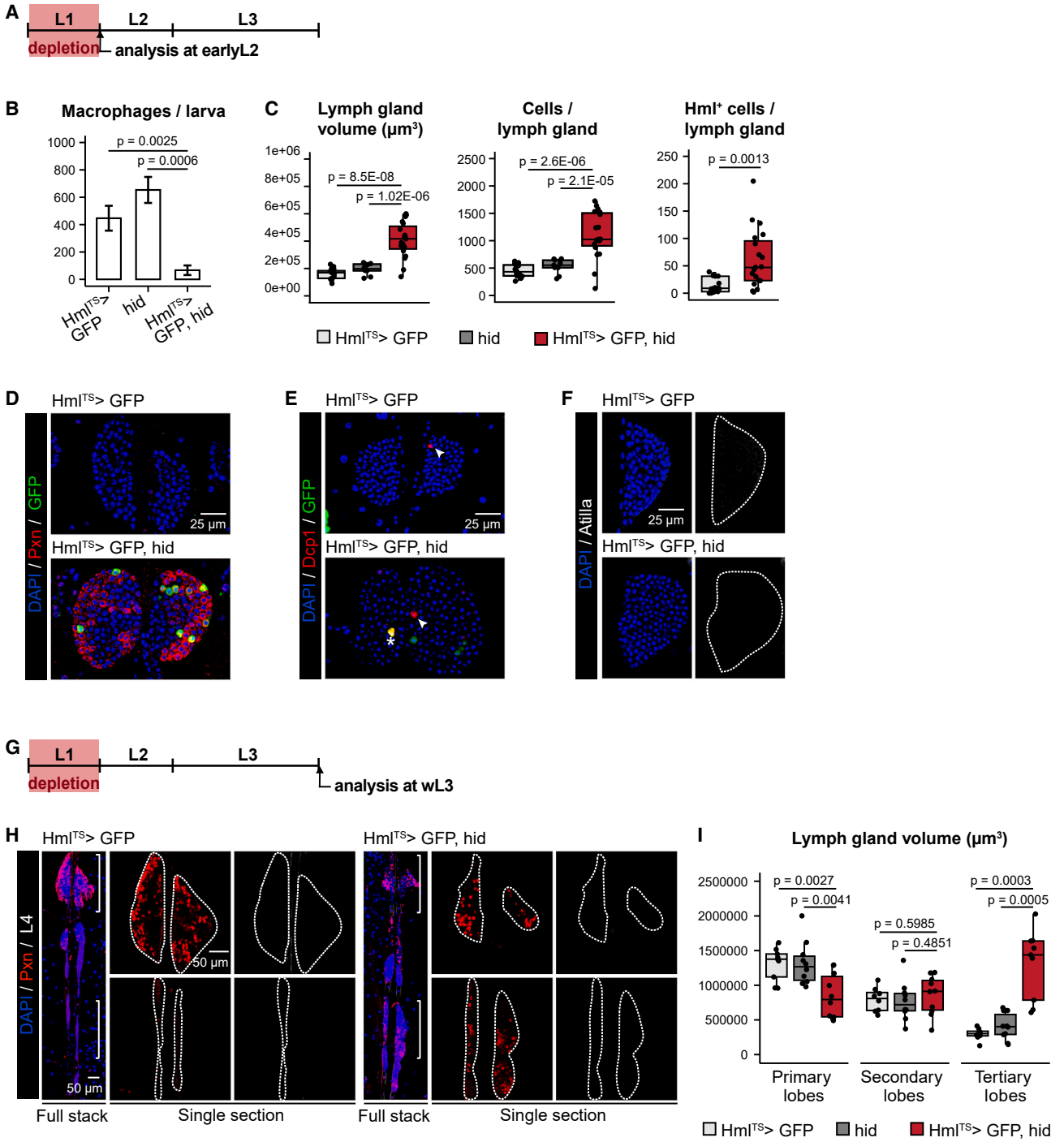

Figure 3. Fly EM depletion accelerates the physiological development of the lymph gland

(A) Experimental setup adopted in (B)–(F). The genetic depletion was restricted to the first larval instar (L1) using a thermosensitive inhibitor of Gal4 (*tubulinGal80^{TS}*), active at 18°C and inactive at higher temperature (≥25°C). Embryos and L1 larvae were raised at 25°C to trigger the expression of *hid* and reporter GFP under the control of *HmlΔGal4* and (B–F) analyzed right after depletion at earlyL2 (~48 h AEL) or (H–I) shifted at 18°C at earlyL2 (~48 h AEL) to avoid further macrophage depletion and analyzed at wandering third larval instar (wL3) ~120 h AEL.

(B) Number of macrophages per larva (mean ± SD) assessed by brightfield counting (N ≥ 3).

(C) Lymph gland primary lobes' volume, number of cells and Hml^{+} cells (N ≥ 11).

(D–F) Lymph gland immunolabeling with (D) anti-Pxn in red and anti-GFP in green (N ≥ 11), (E) anti-Dcp1 in red and anti-GFP in green (N ≥ 6), and (F) anti-Atilla in gray (N ≥ 6); nuclei are labeled with DAPI in blue. In **(E),** arrowheads point Dcp1^{+} Hml^{-} cells, and the asterisk indicates a Dcp1^{+} Hml^{+} cell.

(G) Experimental setup adopted in (H) and (I).

(legend continued on next page)

processes or to accelerated physiological development, we depleted EMs only before *Hml* is expressed in the lymph gland and in a time-restricted fashion, using a thermosensitive Gal4 inhibitor (*tubulinGal80^{TS}*). Animals were raised at 25°C (*tubulinGal80^{TS}* not active) throughout L1 to induce cell death in EMs, then shifted at 18°C (*tubulinGal80^{TS}* active) at earlyL2 to avoid expression of *hid* in the Hml^{+} cells that start differentiating in the lymph gland. Larvae were analyzed at earlyL2 (i.e., before the temperature shift) (Figures 3A–3F) and at wL3 (Figures 3G–3I). At earlyL2, the EM pool is reduced to less than 20% (Figure 3B), and the lymph gland already shows overgrowth compared with controls (Figures 3C–3F). Enhanced LM differentiation is also observed, with increased Hml^{+} and/or Pxn^{+} cells mostly located in the cortical zone (Figures 3C and 3D), indicating preserved lymph gland patterning. Importantly, we do not detect apoptosis or inflammation in the lymph gland of depleted larvae (Figures 3E and 3F). With regard to the hemolymph, no lamellocytes were detected upon bleeding and brightfield counting (3 independent replicates), and RT-qPCR assays on the bled macrophages did not reveal any increase in the expression level of the pro-inflammatory cytokines Upd2 and Upd3[49,50] upon depletion (Figures S2E and S2F). Thus, early postembryonic EM depletion is sufficient to trigger premature, yet physiological, lymph gland maturation without inducing evident inflammation.

Then, we asked whether the accelerated development persists also at a later stage, leading to precocious rupture of the wL3 lymph gland, or whether it is rescued by compensatory processes. Notably, albeit still present, the primary lobes of the wL3 lymph gland are partially histolyzed (therefore smaller) in the depleted larvae, and the posterior lobes are oversized and more differentiated (Figures 3H and 3I). In line with the ongoing histolysis, the deficit of hemolymph macrophages observed at earlyL2 (Figure 3B) is compensated by wL3 (Figures S2G and S2H). These phenotypes resemble those observed upon constitutive EM depletion (Figures S1C and S1E–S1H). Yet, while the latter protocol triggers inflammation, as evidenced by the presence of lamellocytes (Figures S1H and S1I), lamellocytes are absent in the lymph gland (Figure 3H) and in the hemolymph (brightfield counting, 3 independent replicates) upon L1-restricted depletion.

In sum, the lack of EMs during the early maturation period of the lymph gland accelerates late hematopoiesis.

Murine EM depletion leads to an increased contribution of HSCs to the macrophage pools

The presence of sequential waves of hematopoietic progenitors during development from invertebrates to mammals[51] prompted us to ask whether the interaction observed in *Drosophila* between hematopoietic waves is an evolutionarily conserved process. Hence, we assessed whether murine EMs control HSC-dependent hematopoiesis (Figure 1A). To achieve EM depletion, pregnant dams were fed with CSF1R inhibitor Plexxikon 5622[52] (PLX)-containing chow between E11.5 (after HSC emerge from the aorta) and E14.5, when hematopoiesis is active in the mouse FL (Figure 4A). PLX treatment efficiently depleted EMs by inducing apoptosis in the E14.5 FL (Figures 4B and S7A), while the number of lineage-traced HSC-dependent macrophages (LM) was unaffected (Figures 4C–4E). EM depletion *in utero* did not lead to increased inflammation[53] (Figure S5A). Rather, key inflammation pathways were downregulated in the E14.5 FL (*Tnf*, *Ifn gamma*, *Il1a/b*, *Il18*, and *Il10*), while negative regulators of cytokine signaling (*Socs1&2*) were upregulated.

After withdrawal of CSF1R inhibition, macrophages rebound to control numbers 48 h after (E16.5) in FL and 96 h after (E18.5) in brain and skin (Figures 4C–4E, upper panel). The specific contribution of late-wave (HSC-derived) hematopoiesis was investigated in *Cdh5^{CreERT2} Rosa26^{Tomato}* embryos pulsed at E10.5 with 4OHT (Figure 4A), which labels endothelial cells after E10.5, including the hemogenic endothelium giving rise to HSCs.[54] An increased HSC contribution (measured by the labelling efficiency of macrophages) was observed as early as E14.5 and maintained throughout development in PLX-treated FL (Figures 4C and 4D, middle panel). HSC contribution to peripheral tissue macrophages increased 2 days later than in FL, at E16.5. The number of LM in FL and brain increased dramatically between E14.5 and E16.5 and was stable between E16.5 and E18.5 (Figures 4C and 4D, lower panel). In contrast to skin and FL, there was only a transient HSC contribution to brain macrophages (microglia), in line with the moderate fetal HSC contribution to microglia pools.[55]

The contribution of surviving EMs to the repopulation was quantified in *Cdh5^{CreERT2} Rosa26^{tdTomato}* embryos pulsed at E7.5 to distinguish EMs (EMP-derived, Tomato positive) from LMs (Tomato negative). At E16.5, both EMs and LMs proliferate and contribute to the repopulation of macrophage pools in the FL and brain, albeit at different extents (Figure S5G). This may explain why macrophage numbers overshot at E18.5, both in the brain and FL, but returned to normal numbers by 6 weeks after birth (Figures 4C–4E, upper panel).

Surprisingly, HSC contribution to resident macrophages decreased over time to return to control levels in adulthood. In all three organs, the labeling efficiency of liver Kupffer cells, brain microglia, and epidermal Langerhans cells was not different between offspring from control and PLX-treated dams. This suggests that although HSC-derived LMs outperform EMs in their proliferative capacity in the acute recovery phase after PLX, they are incapable of long-term self-maintenance and are hence eventually replaced by EMs.

Monocytes, often viewed as macrophage precursors, were unaffected in FL, brain, and blood at the end of the PLX treatment (Figures 4F–4H, upper panel), as were neutrophils, also produced during both early- and late-wave hematopoiesis (Figures S5C and S5D). In regard to their ontogeny, HSC contribution to circulating monocytes and neutrophils was barely detectable at E14.5 in control and PLX-treated embryos

(H) Lymph gland immunolabeling with anti-Pxn in red and the anti-L4 lamellocyte marker in gray; nuclei labeled with DAPI in blue. Brackets indicate the lobes represented in the blow-up, and dashed lines mark the perimeter of the lymph gland lobes (N ≥ 8).
(I) Lymph gland lobes' volume (N ≥ 9). Detailed genotypes: *w;HmlΔHmlΔGal4,UAS-2XEGFP/+;tubGal80^{TS}/+* (Hml^{TS} > GFP), *w;UAS-hid/+* (hid), *w;HmlΔGal4,UAS-2XEGFP/UAS-hid;tubulinGal80^{TS}/+* (Hml^{TS} > GFP, hid). Confocal images are shown as representative single sections unless otherwise specified. Statistics: two-tailed unpaired t test.

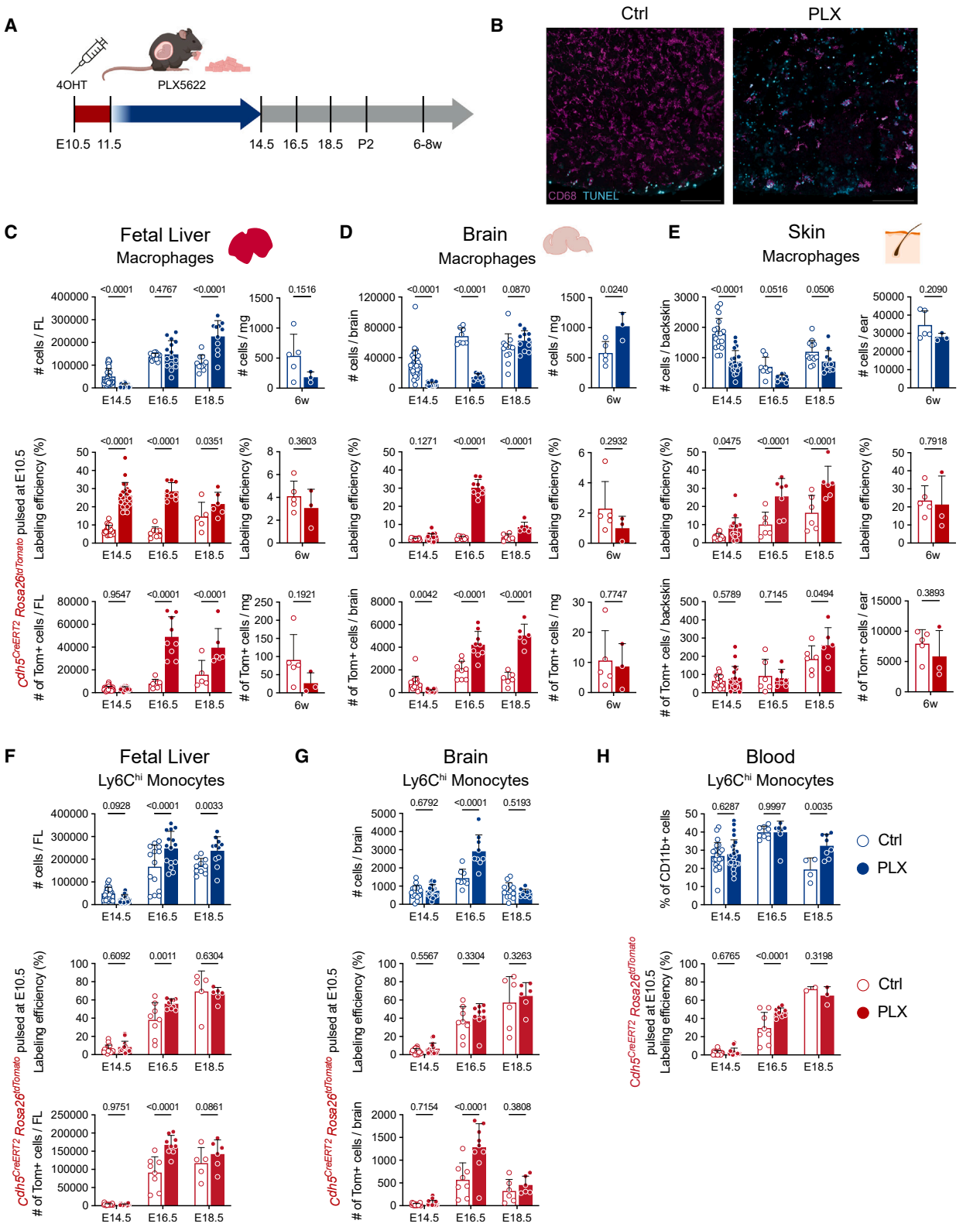

Figure 4. Murine EM depletion leads to an increased contribution of HSCs to macrophage pools

(A) *Cdh5*^{CreERT2} *Rosa26*^{tdTomato} pregnant dams were pulsed with 4OHT at E10.5 to lineage trace hematopoietic progenitors born from endothelium after E10.5 and placed the next day on control (Ctrl) or CSF1R inhibitor-containing chow (PLX5622, PLX) for 3 days. Hematopoiesis was then assessed on the last day of CSF1R inhibition (E14.5) and after withdrawal of CSF1R inhibition.

(legend continued on next page)

(Figures 4F, S5C, and S5D, respectively). During the PLX recovery phase, HSC contribution to Ly6C^{hi} monocytes increased at E16.5 in the blood and FL of PLX-treated embryos and plateaued at E18.5 with controls (Figures 4F–4H, middle panel), having reached the maximum efficiency of the system. Thus, HSC produced larger numbers of monocytes ahead of time after EM depletion (Figures 4F and 4G, lower panel). Furthermore, increased monocyte output by HSCs in EM-depleted embryos was not short lived, and Ly6C^{hi} monocytes were increased in blood at E18.5 and after birth (post-natal day [P] 2) but were back to control values by 8 weeks (Figure S4E). Notably, the 2-fold increase in FL monocytes was detected 2 days after the doubling in size of the FL macrophage population (Figures 4C and 4F), suggesting that the increase in monocyte numbers is not due to an overcompensation to repopulate macrophage pools in peripheral tissues or FL but rather the read-out of a more global change in late-wave hematopoiesis. Similarly, the contribution of late-wave hematopoiesis to neutrophils was increased in FL at E16.5, which resulted in increased neutrophil numbers at E18.5 (Figure S5C), indicating an overproduction of neutrophils that accumulate in the FL. While blood neutrophils were unaffected throughout development, in ontogeny and frequency (Figure S5D), neutrophil numbers were increased in blood after birth and at P2 but were back to control values in adulthood (Figure S5F).

Altogether, these data suggest enhanced or accelerated HSC differentiation toward monocytes and neutrophils after transient depletion of EM macrophages *in utero*. Thus, murine EM depletion drives an earlier contribution of HSC hematopoiesis to myeloid cells (neutrophils, monocytes, and macrophages) as in *Drosophila*.

Murine EM depletion triggers precocious HSC commitment and differentiation

To assess how HSC-derived hematopoiesis was affected by the loss of EMs, we quantified the number of progenitors in the E14.5 FL after EM depletion. Within the Lin neg Sca1+ Kit+ (LSK) compartment, short-term (ST-) HSCs,[56] as well as lymphoid-biased multi-potent progenitors (MPP4), were not affected. In contrast, long-term (LT-) HSCs and erythroid-biased MPPs (MPP2) were upregulated, while myeloid-biased MPPs (MPP3) were reduced in numbers. These changes were only transient, and progenitor populations were back to control levels by E18.5, except for MPP2 (Figures 5A and 5B). This demonstrates that HSC-derived hematopoiesis is altered by EM depletion and suggests an increased commitment of HSCs into downstream progenitors. To investigate this further, we characterized committed myeloid progenitors. The differentiation cascade in early-wave (from EMPs) and late-wave (from HSC) hematopoiesis toward myeloid cells is summarized in Figure 5A. By E14.5, the progenitors upstream of the myeloid differentiation cascade (common myeloid progenitors [CMPs] and granulocyte-monocyte progenitor [GMP]) are significantly increased in numbers, while more committed downstream progenitors (macrophage/dendritic cell progenitor [MDP], common monocyte progenitor [cMoP]) are unaffected (Figure 5C). Intriguingly, not only myeloid progenitors but also megakaryocyte-erythroid progenitors (MEPs) were increased in numbers at E14.5 (Figure S6C). The changes in progenitors persisted until E18.5 in the FL. Thus, PLX treatment does not deplete hematopoietic progenitors, instead it enhances progenitor production.

Moreover, EM depletion leads to long-lasting changes in HSC-derived hematopoiesis. Bone marrow (BM) colonization by HSCs at P2 was unaffected in EM-depleted embryos (Figure S6D). While most progenitor cell numbers were unchanged, lymphoid-biased MPP4 were reduced at P2 and in adulthood (Figures S6D and S6E). Furthermore, when single CMPs from adult (6–8 weeks) BM (Figures 5D and 5E) were sorted and cultured for 7 days in liquid culture, they produced larger macrophage and neutrophil colonies if they had undergone transient EM depletion *in utero*. Although tissue macrophages, circulating monocytes, and neutrophil numbers in adult mice were normal (Figures 4C–4E, S5E, and S5F), these results show a long-term increased myeloid differentiation potential of HSC-derived progenitors after transient macrophage depletion in the developmental period at the expense of lymphoid potential.

The acceleration of late hematopoiesis caused by fly EM depletion does not rely on inflammation or on EM phagocytic ability

EM depletion causes acceleration of late hematopoiesis in both flies and mice, suggesting that layered hematopoiesis plays an important and conserved function in adjusting immune system development. Next, we asked what the underlying mechanisms are, and we first took advantage of the fly model to narrow down the specific macrophage function at play.

To further exclude the involvement of inflammation, we reduced the EM number by preventing their proliferation. The String/Cdc25 (Stg) tyrosine protein phosphatase required for cell-cycle progression[57] was knocked down in EMs by expressing a *stg RNAi* transgene[58] under the control of *HmlΔGal4* until midL2, when lymph glands were analyzed (Figures 6A–6G).

(B) Representative immunolabeling of E14.5 fetal livers from control and PLX-treated embryos. Anti-CD68 (macrophages, magenta); TUNEL (cyan). Scale bar represents 100 μm.
(C) Number of CD45+ CD11b+ F4/80+ CD64+ Tim4+ macrophages (top), frequency (middle), and number (bottom) of tdTomato+ fetal liver macrophages per fetal liver or per mg of 6-week-old adult liver.
(D) Number of CD45+ CD11b+ F4/80+ CD64+ macrophages (top), frequency (middle), and number (bottom) of tdTomato+ macrophages per fetal brain or per mg of 6-week-old adult brain.
(E) Number of CD45+ CD11b+ F4/80+ CD64+ macrophages (top), frequency (middle), and number (bottom) of tdTomato+ macrophages per fetal backskin or per ear skin epidermis of one ear of 6-week-old adults.
(F and G) Number of CD45+ CD11b+ F4/80- Ly6Chi monocytes (top), frequency (middle), and number (bottom) of tdTomato+ monocytes per fetal liver (F) and brain (G).
(H) Frequency of CD115+ Ly6Chi monocytes among blood CD11b+ cells (top) and frequency of tdTomato+ blood Ly6Chi monocytes (bottom). (C–H) Mean ± SD; control (Ctrl, blue border) and macrophage-depleted (PLX, blue fill) embryos. Symbols correspond to individual embryos from at least two independent litters per time point and per treatment group. Tukey multiple comparisons test (embryos) and unpaired t test (adults).

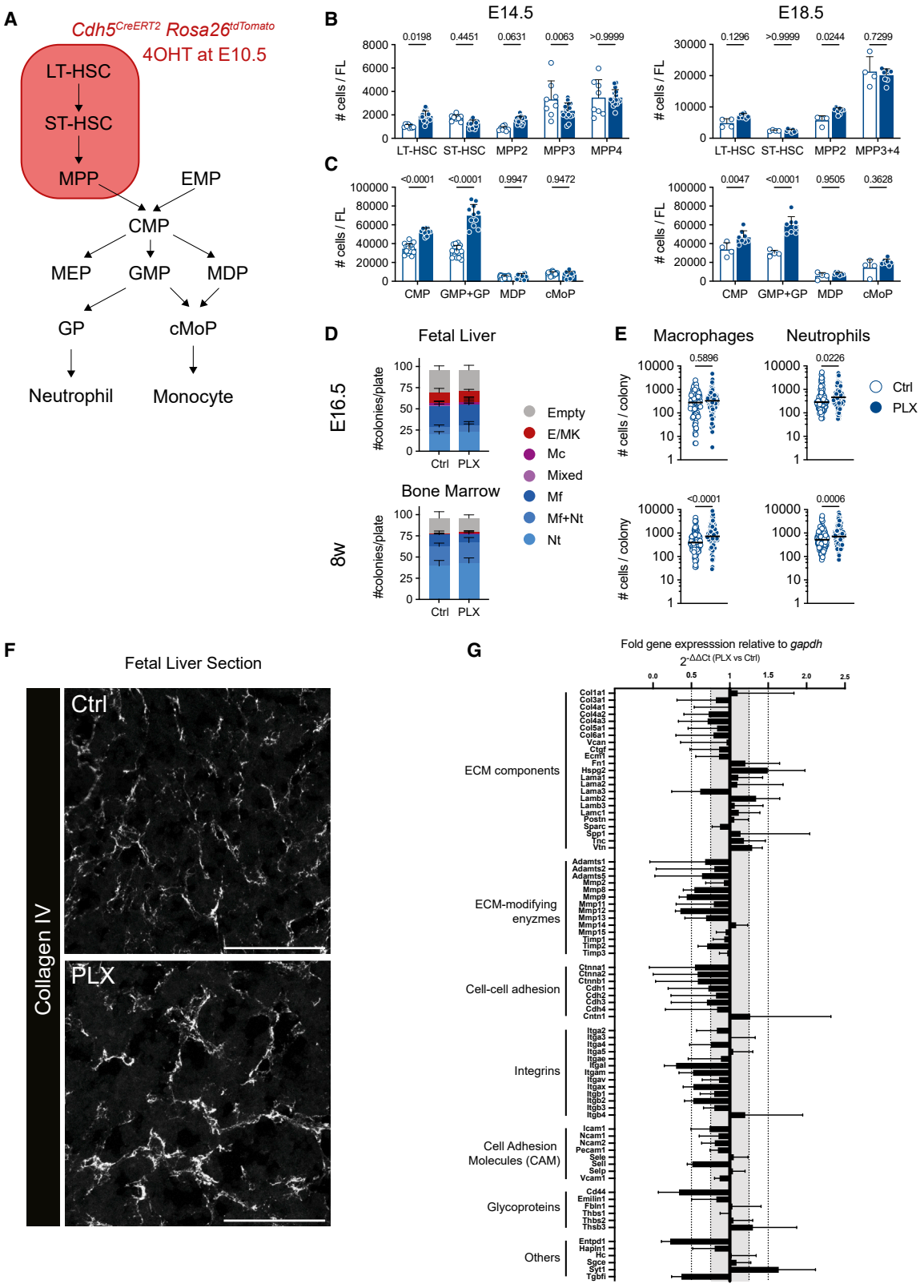

Figure 5. Murine EM depletion alters fetal liver hematopoiesis and ECM organization

(A) Simplified representation of myeloid commitment and differentiation from definitive multipotent progenitors toward neutrophil and monocyte fates. A 4OHT pulse at E10.5 in *Cdh5*^{CreERT2} *Rosa26*^{tdTomato} embryos labels hematopoietic stem and progenitor cells emerging after E10.5 (red square) and their progeny.

(legend continued on next page)

This strategy avoids inducing *stg RNAi* in lymph gland Hml^{+} cells and allows the comparison with midL2 lymph glands dissected after EM depletion (Figures 2G–2J). Upon *stg RNAi*, the number of EMs per larva drops drastically, similar to what observed upon depletion (Figures 6B and 2C). However, while EMs are barely detectable by immunolabeling upon depletion (Figures 2D and 2E), EMs from *stg RNAi* larvae have normal morphology and are mostly Hml^{-}, and their numbers are in accordance with those obtained by brightfield counting (Figure 6C). This likely accounts for the milder phenotype induced by *stg RNAi* compared with that induced by cell depletion (see below). No lamellocytes were detected by brightfield counting (4 independent replicates), indicating the absence of inflammatory states. Even in these conditions, however, the lymph gland is increased in size and shows precocious cell differentiation, mostly in the cortical zone (Figures 6D and 6E), without signs of apoptosis or inflammation (Figures 6F and 6G) as in the L1-restricted depletion (Figures 3E, 3F, and 3H).

Since the accelerated lymph gland development triggered by EM loss does not rely on inflammatory mechanisms, a specific EM function, namely phagocytosis and/or secretion, might be involved. Downregulating the expression of the phagocytic receptor Eater in EMs (*eater RNAi*[59] expressed under the control of *HmlΔGal4*) does not impact EM number or accelerate lymph gland development at midL2 (Figures 6H–6K), suggesting that the EM phagocytic function does not underlie the modulation of late hematopoiesis.

ECM molecules from fly EMs control lymph gland development

In the lymph gland, cells are interweaved with ECM that also separate the organ from the hemolymph.[28,38,41,60] ECM integrity is crucial for proper cell-cell interactions and to convey homeostatic signaling regulating progenitor maintenance/differentiation. Animals mutant for the ECM component *trol* (ortholog of the mammalian Perlecan) show severe defects in the lymph gland ECM along with precocious differentiation of the organ.[60] EMs produce and secrete several ECM molecules[61,62] such as Trol,[63] the collagen IV subunits Col4alpha1[64] and Viking/Col4alpha2,[65] laminin,[66] and SPARC.[67] We hence asked whether EMs modulate late hematopoiesis through the ECM pathway

We knocked down the expression of Trol in EMs by expressing a *trol RNAi* (Figure S4A) under the control of *HmlΔGal4* until midL2 (before massive differentiation of Hml^{+} cells in the lymph gland), and we analyzed the lymph gland phenotype (Figure 7A). *trol RNAi* triggers a significant increase of the lymph gland volume, along with increased lymph gland cellularity and LM differentiation (Figures 7B and 7C). Similar results were obtained upon knocking down *vkg* (*vkg RNAi*) in EMs (Figures S3A–S3C), further proving the involvement of the ECM pathway in mediating the EM-dependent modulation of late hematopoiesis. The enhanced number of Hml^{+} macrophages observed upon *trol RNAi* may trigger *trol* silencing *in loco*, causing indirect effects. To avoid that, lymph glands were also analyzed at an earlier stage (early-midL2, ~45 h AEL) from larvae raised at 29°C to optimize RNAi efficiency[68] (Figures 7D and S3D). At this stage, no increase of Hml^{+} cells was detected in the lymph glands of *trol RNAi* larvae, yet the organ is already enlarged (Figures 7E, 7F, S3E, and S3F). Of note, *trol* downregulation in EMs does not impinge on the main patterning of the developing lymph gland. At early-midL2, a medullary zone populated by Domeless^{+} (dome) and E-cadherin^{+} (E-cad) progenitors[38,60,69,70] is present and similar to what observed in controls. Furthermore, the precociously differentiated LMs are cortically located, and the PSC, immunolabeled by Antennapedia (Antp),[18] does not show evident defects (Figures 7E,7F, and S3G). Importantly, the patterning is well preserved also at later stages. Upon using the thermosensitive approach to confine *trol* knockdown at L1 and early L2 stages (thus avoiding possible cell autonomous effects) (Figure 7G), in feeding L3 (fL3) lymph glands, we observed a preserved E-cad^{+}, βPS integrin^{+},[71] and wingless^{+} (wg)[22] medullary zone as well as a Pxn^{+} cortical zone at the periphery of the primary lobes (Figures 7H, 7I, S3I, and S3J).

We then assessed the status of the lymph gland ECM of early-midL2 larvae, at the onset of the lymph gland phenotype (Figure 7J). The ECM of controls is clearly organized in a network surrounding single macrophages or small groups of cells. By contrast, this regular architecture is disrupted upon *trol RNAi*: ECM filaments are not properly connected, and wide gaps in the ECM surrounding groups of cells are visible (Figure 7K). Similar defects were scored by immunolabeling the ECM with the anti-Col4alpha1 antibody (Figure S3H). To gain better resolution on the lymph gland ECM structure, we performed transmission electron microscopy (Figure 7L). In control lymph glands, the macrophages appear packed, and the cleft between neighboring cells are generally filled with highly organized ECM filaments. Moreover, the outermost ECM layer coating the lymph gland lobe tightly adheres to the cells in control lymph gland. Upon *trol* downregulation, this external ECM layer is more

LT- and ST- HSCs, long-term and short-term HSCs; MPP, multipotent progenitors; EMP, erythro-myeloid progenitors; CMPs, common myeloid progenitors; MEPs, megakaryocyte-erythroid progenitors; GMP, granulocyte-monocyte progenitor; GP, granulocyte progenitor; MDP, macrophage/dendritic cell progenitor; cMoP, common monocyte progenitor.

(B and C) Number (mean ± SD) of LT-HSC, ST-HSC and MPP2 (CD150+ CD48+ CD135- LSK, erythroid-biased), MPP3 (CD150- CD48+ CD135- LSK, myeloid-biased), MMP4 (CD150- CD48+ CD135+ LSK, lymphoid-biased) (B) and of CMP, GMP + GP, MDP, and cMoP (C) per fetal liver at E14.5 (left) and E18.5 (right). Mean ± SD; control (Ctrl, blue border) and macrophage-depleted (PLX, blue fill) embryos. Symbols correspond to individual embryos from at least two independent litters per time point and per treatment group. Statistics: one-way ANOVA.

(D) Stacked bar charts (mean ± SD) representing the number and types of colonies in CFC assay of CMP from E16.5 fetal liver (top) and 8-week-old bone marrow (bottom). Empty wells, erythrocyte-megakaryocyte- (E/Mk), mast cell- (Mc), mixed- (E/Mk and/or Mc and/or Mf and/or Nt), macrophage- (Mf), neutrophil- (Nt), and neutrophil-macrophage- (Nt + Mf) containing colonies.

(E) Scatter dot plot (median) representing the number of cells (macrophages or neutrophils) in single colonies from E16.5 (top) and adult CMP (bottom). Statistics: Mann-Whitney.

(F) Representative anti-Coll IV (gray) immunolabeling of E14.5 fetal liver from control and PLX-treated embryos. Scale bar represents 100 μm.

(G) Fold gene expression (mean ± SD) relative to *gadph* in E14.5 control and EM-depleted FL.

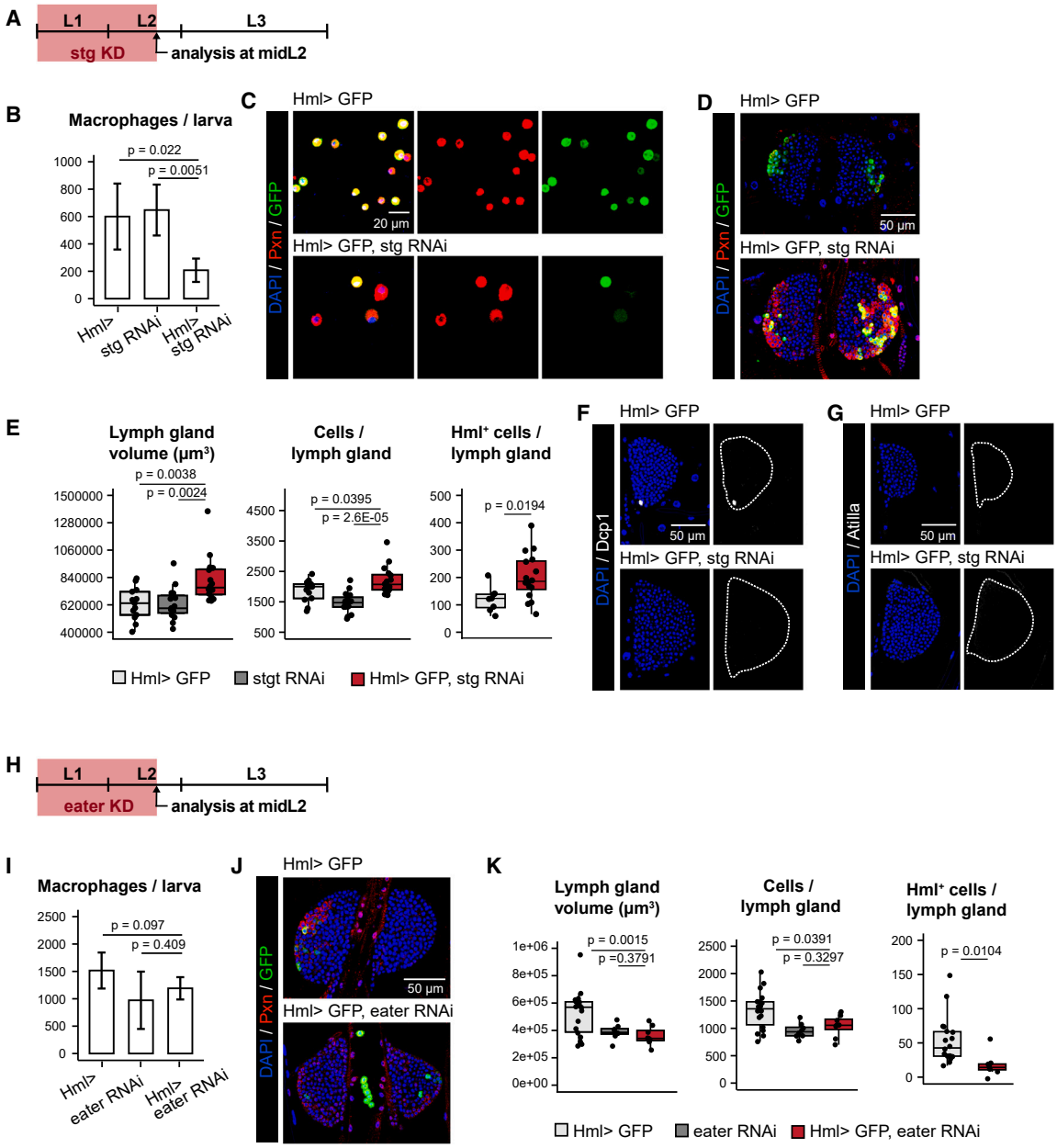

Figure 6. The acceleration of late hematopoiesis caused by fly EM depletion does not rely on inflammation or on EM phagocytic ability

(A) Experimental setup adopted in (B)–(G). The *HmlΔGal4* driver was used to knock down (KD) *string/cdc25* (*stg RNAi*), a positive regulator of cell-cycle progression, in EMs from the beginning of the larval life until midL2 (~65 h AEL) with animals raised at 25°C. *Hml* expression was revealed through a reporter GFP.

(B) Number of macrophages per larva (mean ± SD) assessed by brightfield counting (N ≥ 3).

(C) Immunolabeling of bled macrophages. Anti-Pxn is in red, anti-GFP in green, and nuclei are labeled with DAPI in blue.

(D–F) Lymph gland immunolabeling with (D) anti-Pxn in red and anti-GFP in green (N ≥ 14), (F) anti-Dcp1 in gray (N ≥ 8), and (G) anti-Atilla in gray (N = 6); nuclei are labeled with DAPI in blue. Dashed lines mark the perimeter of the lymph gland lobes. (E) Lymph gland primary lobes' volume, number of cells, and number of Hml^{+} cells (N ≥ 13). Both sexes in a 1:1 ratio were used for the lymph gland analysis upon *stg RNAi*.

(H) Experimental setup adopted in (I)–(K). The phagocytic receptor *eater* was knocked down (*eater RNAi*) in EMs under the control of *HmlΔGal4* from the beginning of the larval life until midL2 (~65 h AEL) with animals raised at 25°C. *Hml* expression was revealed through a reporter GFP.

(I) Number of macrophages per larva (mean ± SD) assessed by brightfield counting (N ≥ 3).

(J) Lymph gland immunolabeling with anti-Pxn in red and anti-GFP in green; nuclei are labeled with DAPI in blue (N ≥ 8).

(K) Lymph gland primary lobes' volume, number of cells and number of Hml^{+} cells (N ≥ 8). Detailed genotypes: *w;HmlΔGal4,UAS-2XEGFP/+;+* (Hml > GFP), *w;stg RNAi/+;+* (stg RNAi), *w;HmlΔGal4,UAS-2XEGFP/stg RNAi;+* (Hml > GFP, stg RNAi), *w;HmlΔGal4/+;+* (Hml>), *w; HmlΔGal4/stg RNAi;+* (Hml > stg RNAi), *w;+;eater RNAi/+* (eater RNAi), *w;HmlΔGal4,UAS-2XEGFP/+;eater RNAi/+* (Hml > GFP, eater RNAi), *w; HmlΔGal4/+;eater RNAi/+* (Hml> eater RNAi). Confocal images are shown as full-stack projections for bled macrophages and representative single sections for lymph glands unless otherwise specified. Statistics: two-tailed unpaired t test.

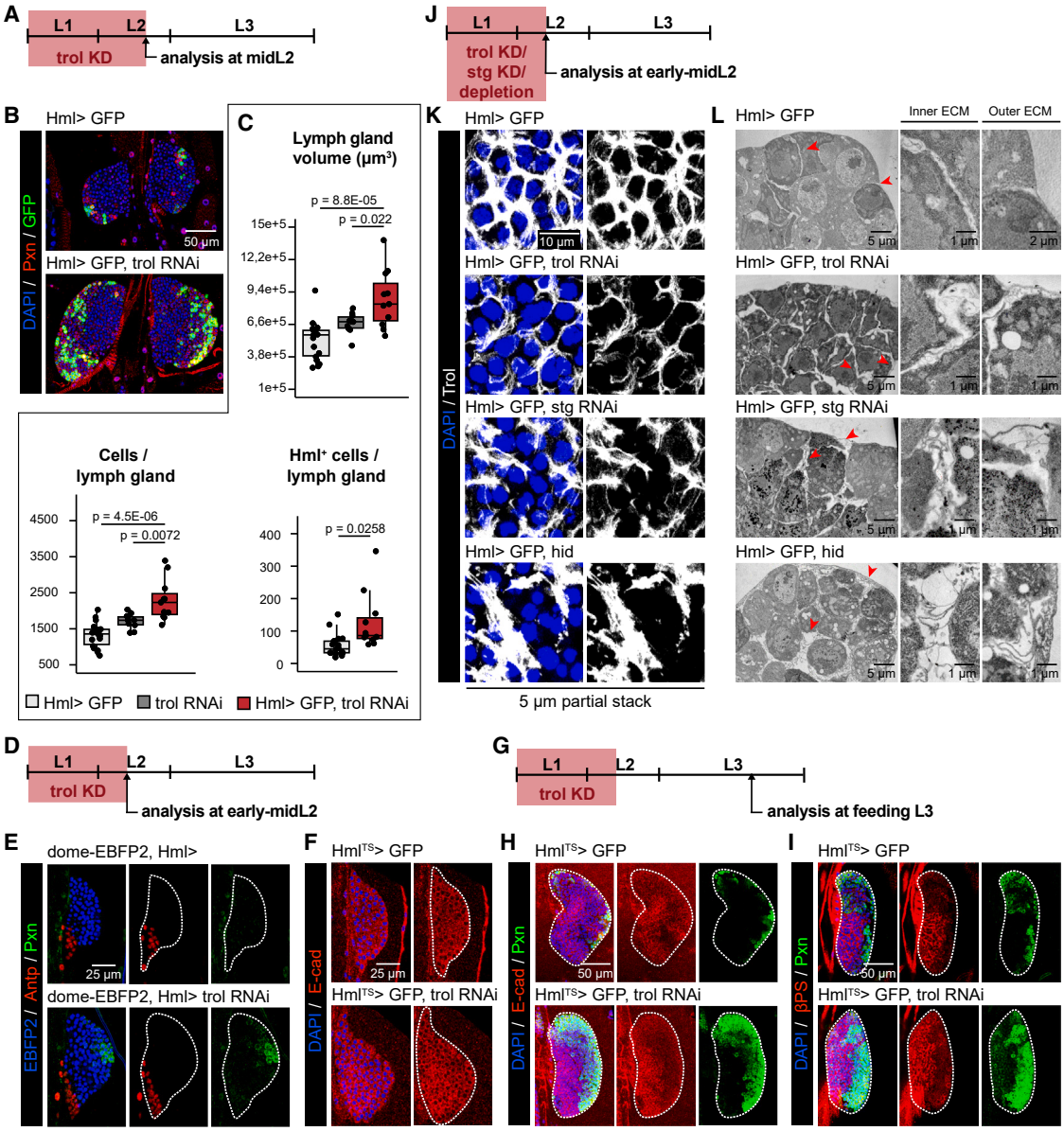

Figure 7. The downregulation of extracellular matrix (ECM) molecules in fly EMs accelerates the lymph gland development and affects the lymph gland ECM organization without altering the patterning

(A) Experimental setup adopted in (B) and (C). The *HmlΔGal4* driver was used to express a reporter GFP and knock down the ECM molecule Trol (*trol RNAi*) in EM from the beginning of the larval life until midL2 (~65 h AEL) with animals raised at 25°C.

(B) Lymph gland immunolabeling with anti-Pxn in red, anti-GFP in green, and nuclei labeled with DAPI in blue. N ≥ 10.

(C) Lymph gland primary lobes' volume, number of cells, and number of Hml^{+} cells in control and *trol RNAi* larvae. N ≥ 10.

(D) Experimental setup adopted in (E) and (F). The *HmlΔGal4* driver was used to knock down *trol* (*trol RNAi*) in EMs from the beginning of the larval life until early-mid second larval instar (early-midL2) ~45 h AEL, with animals raised at 29°C to increase the UAS-Gal4 system efficiency.

(E) Lymph gland immunolabeling in control and *trol RNAi* larvae. A *domeless* reporter labels the medullary zone in blue (EBFP2), the posterior signaling center marker Antp (Antennapedia) is in red, and anti-Pxn in green. N = 6. dashed lines: perimeter of the lymph gland primary lobes.

(F) Lymph gland immunolabeling with the medullary zone marker E-cad in red and nuclei labeled in blue with DAPI. N ≥ 11. Despite the presence of a *tubulinGal80^{TS}*, no temperature shift was performed to reproduce the conditions used in (E).

(G) Experimental setup adopted in (H) and (I). *trol* knock down was restricted to L1 and beginning of L2 using a thermosensitive inhibitor of Gal4 (*tubulinGal80^{TS}*), which is active at low temperature (18°C) and inactive at higher temperature (≥25°C). Embryos and larvae were raised at 29°C until early-midL2 (~45 h AEL) to trigger *trol* knock down and expression of a GFP reporter under the control of the Hml. Then, animals were shifted at 18°C and analyzed at feeding third larval instar (fL3).

(H and I) Lymph gland immunolabeling with anti-Pxn in green, anti-E-cadherin (E-cad) **(H)** and βPS integrin (βPS) **(I)** in red, and nuclei labeled in blue with DAPI. N ≥ 5.

(legend continued on next page)

convoluted, with gaps between cells or scarce ECM filaments around them. Similar ECM was detected upon downregulating EM proliferation (*stg RNAi*), and it was even more evident upon EM depletion (Figures 7K and 7L).

Overall, these results demonstrate that the secretion of ECM molecules such as Trol and collagen IV by EMs contribute to the integrity of the lymph gland ECM and that the loss of this ECM source accelerates the physiological course of late hematopoiesis.

Murine EM depletion modifies the ECM of the FL niche

We finally probed whether the modulation of HSC hematopoiesis by murine EMs also involved changes in ECM remodeling in the fetal hematopoietic niche, as evidenced in the fly lymph gland. By E14.5, the FL ECM is mostly composed of laminins, nidogen, fibronectin, HSPG, and type IV Collagen.[72] Analysis of E14.5 FL sections revealed changes to the fine structure of the ECM, with a reduction of the Collagen IV network in PLX-treated embryos (Figures 5F and S7B). We thus probed the expression of ECM-related genes and found that out of 79 tested genes, expression of only 4 genes is upregulated (>1.2-fold increase; *Syt1*, *Vtn*, *Lamb2*, and *Hspg2*). In contrast, 40 genes are downregulated (<0.8-fold change), among them ECM key components (Collagens, Laminins, and Versican) and ECM-modifying enzymes (Mmp8, 9, 12, and 13; Adamts 1,2 and 5; and Timp2). Furthermore, several genes coding for key adhesion molecules (belonging to Cadherin, Integrin, and CAM families) are also downregulated in PLX-treated embryos (Figure 5G).

Thus, macrophage depletion between E11.5 and E14.5 leads to profound changes in ECM organization in the E14.5 FL, demonstrating that ECM alteration at the site of late hematopoiesis is evolutionarily conserved upon EM depletion.

DISCUSSION

Multiple hematopoietic waves have been observed throughout evolution, and macrophages from different waves co-exist during development and then adult life.[73] This has sparked a renewed interest in macrophage function during tissue repair, infection, and tumor growth[74–85] in light of their two possible origins and maintenance mechanisms: prenatal EMs that self-renew versus continuously recruited HSC-derived macrophages. Although macrophages from early waves colonize the embryo including the hematopoietic niches, little is known about their developmental function in late hematopoietic waves. Since these macrophages experience varied physiological/pathological stimuli, we asked whether homeostatic interactions occur between the different waves as an evolutionarily conserved mechanism to adjust late hematopoiesis and ensure a proper blood cell repertoire. We here identify EMs as key regulators of late hematopoiesis throughout evolution, and we uncover the ECM as an important mediator of the process. Our study demonstrates that EMs work as signaling hubs for HSC-dependent hematopoiesis.

EMs control late hematopoiesis

Drosophila LMs are generated in the lymph gland, whose development is tightly regulated by well-described signals exchanged between PSC (the signaling niche), progenitor cells, and mature LMs (reviewed in Banerjee et al.[16]). Organs outside the lymph gland, i.e., cardiac tube, brain, and fat body (equivalent to the mammalian liver), also contribute to the process.[86–89] Here, we reveal EMs as an additional source of cues regulating lymph gland maturation under physiological conditions. The constitutive loss of EMs not only boosts growth and LM differentiation in the lymph gland but also results in increased cell death and the presence of activated immune cells. This is due to an indirect effect rather than being triggered by EM loss, as LMs precociously expressing *Hml* in the lymph gland die and trigger the inflammatory state. By contrast, the analysis of early-stage lymph glands upon EM depletion already displays increased cell proliferation and precocious cell differentiation, in the absence of apoptosis and lamellocytes. Moreover, similar phenotypes are triggered by decreasing EM proliferation. Thus, the loss of EMs at the beginning of lymph gland development accelerates a bona fide physiological maturation of the lymph gland, which maintains a wild-type-like patterning.

Previous works hint at the involvement of embryonic macrophages in modulating vertebrate late hematopoiesis. Zebrafish embryonic macrophages facilitate the entry of HSCs into circulation from their site of emergence, whereas murine embryonic macrophages participate to the emergence of HSCs from the aorta-gonado-mesonephros region.[15,90] Here, we reveal the role of EMs in HSC expansion and differentiation. Inhibition of signaling downstream of the main macrophage growth factor receptor (CSF1R) during embryonic development leads to macrophage depletion, without affecting CSF1R+ hematopoietic progenitors or monocytes. After withdrawal of CSF1R inhibition, macrophages return to normal levels, first in the FL and then in peripheral tissues (brain and skin). However, EM depletion profoundly impacts fetal HSC behavior. Macrophage repopulation from HSC-derived cells was driven by the increase in HSC differentiation into erythro-myeloid cells. Of note, the few LMs present at E14.5 surviving the treatment could also contribute to the repopulation through local proliferation. Thus, HSC commitment and differentiation into myeloid cells, not only

(J) Experimental setup adopted in (K) and (L). The *HmlΔGal4* driver was used to knock down *trol* (*trol RNAi*) or *stg* (*stg RNAi*) or express the cell death gene *hid* in EMs from the beginning of the larval life until early-midL2 (~45 h AEL, animals raised at 29°C).

(K) Lymph gland immunolabeling in control (N ≥ 10), *trol RNAi* (N ≥ 10), *stg RNAi* (N ≥ 6), or depleted larvae (N ≥ 6). Anti-Trol is in gray, and nuclei are labeled with DAPI in blue.

(L) Transmission electron microscopy micrographs of lymph glands from control, *trol RNAi*, *stg RNAi*, or depleted larvae. Low magnified images are on the left, and red arrowheads point the fields represented at higher magnification on the right, which are centered on the inner or outer lymph gland ECM. Detailed genotypes: *w;HmlΔGal4,UAS-2XEGFP/+;+* (Hml > GFP), *w;+;trol RNAi/+* (trol RNAi), *w;HmlΔGal4,UAS-2XEGFP/+;trol RNAi/+* (Hml > GFP, trol RNAi), *w;HmlΔGal4,UAS-2XEGFP/stg RNAi;+* (Hml > GFP, stg RNAi), *w;HmlΔGal4,UAS-2XEGFP/UAS-hid;+* (Hml > GFP, hid), *w,domeMeso-EBFP2/+;HmlΔG4/+* (dome-EBFP2, Hml>), *w,domeMeso-EBFP2/+;HmlΔG4/+;trol RNAi/+* (dome-EBFP2, Hml > trol RNAi), *w;HmlΔGal4,UAS-2XEGFP/+;tubulinGal80TS/+* (HmlTS > GFP), *w;HmlΔGal4,UAS-2XEGFP/+;tubulinGal80TS/trol RNAi* (HmlTS > GFP, trol RNAi). Confocal images are shown as representative single sections unless otherwise specified. Statistics: two-tailed unpaired t test.

monocyte/macrophages but also neutrophils, is accelerated. In contrast to the limited differentiation of HSCs into myeloid cells at E14.5 in unperturbed development, EM depletion leads to an earlier contribution of HSCs to upstream multipotent and myeloid progenitors. 4 days after the withdrawal of CSF1R inhibition, increased myeloid output of HSC is evidenced by the doubling of myeloid progenitors (GMPs and granulocyte progenitors [GP]), monocytes, and neutrophils in the FL. Importantly, the increased myeloid-bias of HSCs is still present in the post-natal and adult bone marrow, raising important questions on the long-lasting contribution of pre-natal challenges into adult homeostasis, such as how the hematopoietic system of PLX-treated offspring would respond to secondary challenges.

Despite the different cellular hematopoietic mechanisms linked to specific developmental schemes and lifespan extent (lack of extraembryonic and adult hematopoiesis in flies) between flies and vertebrates, our findings strengthen the hypothesis that layered hematopoiesis is a beneficial strategy that the organism has adopted to face the different environments and needs encountered during development.

ECM components secreted by EMs regulate late hematopoiesis

In flies, the appropriate deposition of the ECM throughout the organ is essential for lymph gland development. It ensures proper local environments, allowing cell-to-cell interactions and controlled diffusion of signals that regulate progenitor maintenance/differentiation. *trol*/*Perlecan* encodes an heparan sulfate proteoglycan of the ECM, and its silencing in lymph gland progenitors leads to a mild increase of LM differentiation at late larval stage. This phenotype is much more severe when *trol* is downregulated ubiquitously,[60] suggesting that additional sources of ECM proteins impinge on lymph gland development. Here, we show that EM-derived ECM molecules contribute to lymph gland maturation. Knocking down *trol* or *viking* (a Collagen IV subunit) expression in EMs leads to defective ECM organization in early-stage lymph gland and accelerates lymph gland growth and differentiation while preserving organ patterning, similar to what we observed upon EM loss. These phenotypes cannot be explained by cell autonomous effects, since *trol* mutation or downregulation in the lymph gland does not phenocopy our results.[60] The involvement of pathways other than the ECM in the regulation of late hematopoiesis by EMs cannot be excluded, but the EM function at play is most likely the secretory one, since reducing the expression of the phagocytic receptors Eater does not have evident impact on the lymph gland.

We did not discriminate between direct and indirect effects on the lymph gland in this study. Nevertheless, we searched for a potential role of macrophages in depositing Trol on the fat body, which is close to the lymph gland and is known to be a signaling hub. Upon overexpressing Trol in EMs (Figure S4A), we could observe a more refined Trol pattern in the fat body compared with controls (Figures S4B and S4C), calling for possible indirect effects. The fact that the phenotype is not 100% penetrant underlines again the complexity of the process, which may involve additional tissues. Of note, Trol overexpression in EMs induced lymph gland phenotypes similar to those induced by *trol* knockdown (Figure S4D), indicating that it is the balance of the Trol molecule that matters.

The mouse model does not allow dissecting different macrophage functions (phagocytosis/secretion). Thus, benefiting from the hypothesis tested in the fly larva, we could show that embryonic macrophage depletion in mice also leads to profound changes in the hematopoietic niche ECM. The FL ECM in depleted embryos shows downregulation of key ECM components (e.g., type IV Collagen, Laminins). In regard to ECM production by macrophages, available RNA-seq datasets of embryonic liver macrophages[91] show the expression of several collagen family members (*Col1a1*, *Col3a1*, *Col4a1-2*, *Col5a1-2*, and *Col6a1-2*) and other ECM genes (*Lama3*, *Sparc*, and *Spp1*), all of which are downregulated in the E14.5 FL upon macrophage depletion. In contrast, while embryonic liver macrophages do express *Hspg2, Vtn*, and *Fn1*, overall expression of these genes in EM-depleted FL is upregulated, suggesting compensatory mechanisms by other liver populations. *Vtn* and *Fn1* are expressed by fetal hepatocytes.[92] In addition, embryonic macrophages express several key ECM-modifying enzymes during development from the Adamts, Timp, and MMP families, thus suggesting that depletion of embryonic macrophages could lead to changes not only in the ECM composition but also in its organization or ability to present/release growth factors and cytokines. Importantly, there appears to be a global dysregulation of cell-cell and cell-ECM adhesion, as evidenced by the downregulation of integrin genes, E-cadherin (*Cdh1*), N-cadherin (*Cdh2*), cadherins 3 and 4, and downstream catenins that connect them to the actin cytoskeleton. Thus, whether murine EMs are a cellular source for ECM components, are involved in ECM remodeling, or rather have an indirect effect through crosstalk with other FL cell populations needs to be further explored.

In sum, the acceleration of LM differentiation upon EM depletion is evolutionarily conserved, and we disclose the ECM pathway as an important mediator of this process. The role of EMs in controlling late hematopoiesis improves the current knowledge of the homeostatic function of macrophages, well beyond immunity. Our findings also open important perspectives to understand the etiology of pediatric diseases and to design therapeutic approaches for diseases involving macrophage dysfunctions.

Limitations of the study

This study discloses the impact of EMs on the late immune system development. Further experiments are required to assess whether this is a direct or indirect effect and to characterize additional tissues and pathways possibly regulating late hematopoiesis.

It is also important to note that two hypotheses still need to be further investigated, (1) the respective contribution to the repopulation of surviving LMs versus newly differentiated LMs from monocytes and (2) the contribution of the change of ontogeny in FL macrophages to the HSC phenotype.

STAR★METHODS

Detailed methods are provided in the online version of this paper and include the following:

- KEY RESOURCES TABLE
- RESOURCE AVAILABILITY

- Lead contact
- Materials availability
- Data and code availability

- EXPERIMENTAL MODEL AND STUDY PARTICIPANT DETAILS
  - Fly lines
  - Mouse lines
- METHOD DETAILS
  - Fly macrophage immunolabeling
  - Lymph gland immunolabeling
  - Image acquisition on fly macrophages and lymph glands
  - Transmission electron microscopy
  - RNA extraction and RT-qPCR on fly macrophages and larvae
  - 4OHT Preparation and Injection
  - Flow Cytometry
  - RNA extraction and quantitative qPCR on mouse fetal liver
  - Fetal liver immunolabeling
  - Fetal Liver TUNEL Assay
  - Proliferation assay
  - Single cell liquid culture
- QUANTIFICATION AND STATISTICAL ANALYSIS
  - Quantification
  - Statistical analysis

SUPPLEMENTAL INFORMATION

Supplemental information can be found online at https://doi.org/10.1016/j.devcel.2024.03.013.

ACKNOWLEDGMENTS

We thank I. Ando, J. Shim, A. González Reyes, and S. Noselli for kindly sharing fly lines and antibodies. In addition, fly stocks obtained from the Bloomington Drosophila Stock Center (NIH P40OD018537) and antibodies from the Developmental Studies Hybridoma Bank (DSHB) created by the NICHD of the NIH and maintained at the University of Iowa (Department of Biology, Iowa City, IA 52242) were used in this study. We thank the Imaging and electron microscopy facility of the IGBMC and N. Massaddeq for technical assistance. This work was supported by INSERM, CNRS, UDS, Ligue Régionale contre le Cancer, Hôpital de Strasbourg, ARC, CEFIPRA, ANR grants and by the CNRS/University LIA Calim. E.G.P. and A.G. were supported by the EMAC ANR PRC grant. S.M. is funded by CEFIPRA, ANR, and FRC; PhD program of Z.A.H. is supported by FRM. The IGBMC was also supported by a French state fund through the ANR Labex. This work of the Interdisciplinary Thematic Institute IMCBio+, as part of the ITI 2021-2028 program of the University of Strasbourg, CNRS, and Inserm, was supported by IdEx Unistra (ANR-10-IDEX-0002) and by SFRI-STRAT'US project (ANR-20-SFRI-0012) and EUR IMCBio (ANR-17-EURE-0023) under the framework of the France 2030 Program. We appreciate the technical support of the Institut Pasteur core facilities, notably the cytometry platform (UTECHS CB) and the Center for Animal Resources and Research. We thank P. Dardenne, Y. Lallemand, C. Guichen, and M. Peixoto for their technical support. This work was also funded by Revive (Investissement d'avenir; ANR-10-LABX-0073) and the European Research Council ERC investigator award (2016-StG-715320 to E.G.P.).

AUTHOR CONTRIBUTIONS

S.M., A.S., P.C., A.G., and E.G.P. designed the experiments; S.M., A.G., A.S., and E.G.P. co- wrote the manuscript; S.M., Z.A.H., and C.D. performed the experiments in *Drosophila*; A.S., C.G.R., and K.A. performed the experiments in mice.

DECLARATION OF INTERESTS

The authors declare no competing interests.

Received: July 6, 2023
Revised: January 8, 2024
Accepted: March 7, 2024
Published: April 2, 2024

REFERENCES

1. Mosser, D.M., Hamidzadeh, K., and Goncalves, R. (2021). Macrophages and the maintenance of homeostasis. Cell. Mol. Immunol. *18*, 579–587. https://doi.org/10.1038/s41423-020-00541-3.
2. Kieusseian, A., Brunet de la Grange, P.B., Burlen-Defranoux, O., Godin, I., and Cumano, A. (2012). Immature hematopoietic stem cells undergo maturation in the fetal liver. Development *139*, 3521–3530. https://doi.org/10.1242/dev.079210.
3. Perdiguero, E.G., and Geissmann, F. (2016). The development and maintenance of resident macrophages. Nat. Immunol. *17*, 2–8. https://doi.org/10.1038/ni.3341.
4. Bertrand, J.Y., Jalil, A., Klaine, M., Jung, S., Cumano, A., and Godin, I. (2005). Three pathways to mature macrophages in the early mouse yolk sac. Blood *106*, 3004–3011. https://doi.org/10.1182/blood-2005-02-0461.
5. Stremmel, C., Schuchert, R., Wagner, F., Thaler, R., Weinberger, T., Pick, R., Mass, E., Ishikawa-Ankerhold, H.C., Margraf, A., Hutter, S., et al. (2018). Yolk sac macrophage progenitors traffic to the embryo during defined stages of development. Nat. Commun. *9*, 75. https://doi.org/10.1038/s41467-017-02492-2.
6. de Bruijn, M.F., Speck, N.A., Peeters, M.C., and Dzierzak, E. (2000). Definitive hematopoietic stem cells first develop within the major arterial regions of the mouse embryo. EMBO J. *19*, 2465–2474. https://doi.org/10.1093/emboj/19.11.2465.
7. Medvinsky, A., and Dzierzak, E. (1996). Definitive Hematopoiesis Is Autonomously Initiated by the AGM Region. Cell *86*, 897–906. https://doi.org/10.1016/S0092-8674(00)80165-8.
8. Ema, H., and Nakauchi, H. (2000). Expansion of hematopoietic stem cells in the developing liver of a mouse embryo. Blood *95*, 2284–2288. https://doi.org/10.1182/blood.V95.7.2284.
9. Gomez Perdiguero, E., Klapproth, K., Schulz, C., Busch, K., Azzoni, E., Crozet, L., Garner, H., Trouillet, C., de Bruijn, M.F., Geissmann, F., and Rodewald, H.R. (2015). Tissue-resident macrophages originate from yolk-sac-derived erythro-myeloid progenitors. Nature *518*, 547–551. https://doi.org/10.1038/nature13989.
10. Freyer, L., Iturri, L., Biton, A., and Perdiguero, E.G. (2020). Overlapping Definitive Progenitor Waves Divide and Conquer to Build a Layered Hematopoietic System. Preprint at bioRxiv. https://doi.org/10.1101/2020.12.24.424302.
11. Yokomizo, T., Ideue, T., Morino-Koga, S., Tham, C.Y., Sato, T., Takeda, N., Kubota, Y., Kurokawa, M., Komatsu, N., Ogawa, M., et al. (2022). Independent origins of fetal liver haematopoietic stem and progenitor cells. Nature *609*, 779–784. https://doi.org/10.1038/s41586-022-05203-0.
12. Soares-da-Silva, F., Freyer, L., Elsaid, R., Burlen-Defranoux, O., Iturri, L., Sismeiro, O., Pinto-do-Ó, P., Gomez-Perdiguero, E., and Cumano, A. (2021). Yolk sac, but not hematopoietic stem cell-derived progenitors, sustain erythropoiesis throughout murine embryonic life. J. Exp. Med. *218*, e20201729. https://doi.org/10.1084/jem.20201729.
13. Christensen, J.L., Wright, D.E., Wagers, A.J., and Weissman, I.L. (2004). Circulation and Chemotaxis of Fetal Hematopoietic Stem Cells. PLOS Biol. *2*, E75. https://doi.org/10.1371/journal.pbio.0020075.
14. Mikkola, H.K.A., and Orkin, S.H. (2006). The journey of developing hematopoietic stem cells. Development *133*, 3733–3744. https://doi.org/10.1242/dev.02568.

15. Mariani, S.A., Li, Z., Rice, S., Krieg, C., Fragkogianni, S., Robinson, M., Vink, C.S., Pollard, J.W., and Dzierzak, E. (2019). Pro-inflammatory Aorta-Associated Macrophages Are Involved in Embryonic Development of Hematopoietic Stem Cells. Immunity *50*, 1439–1452.e5. https://doi.org/10.1016/j.immuni.2019.05.003.

16. Banerjee, U., Girard, J.R., Goins, L.M., and Spratford, C.M. (2019). Drosophila as a Genetic Model for Hematopoiesis. Genetics *211*, 367–417. https://doi.org/10.1534/genetics.118.300223.

17. Lemos, T., and Merchant, A. (2022). The hedgehog pathway in hematopoiesis and hematological malignancy. Front. Oncol. *12*, 960943. https://doi.org/10.3389/fonc.2022.960943.

18. Mandal, L., Martinez-Agosto, J.A., Evans, C.J., Hartenstein, V., and Banerjee, U. (2007). A Hedgehog- and Antennapedia-dependent niche maintains Drosophila haematopoietic precursors. Nature *446*, 320–324. https://doi.org/10.1038/nature05585.

19. Crisan, M., Kartalaei, P.S., Vink, C.S., Yamada-Inagawa, T., Bollerot, K., van IJcken, W., van der Linden, R., de Sousa Lopes, S.M., Monteiro, R., Mummery, C., and Dzierzak, E. (2015). Monteiro, R., Mummery, C., et al. (2015). BMP signalling differentially regulates distinct haematopoietic stem cell types. Nat. Commun. *6*, 8040. https://doi.org/10.1038/ncomms9040.

20. Pennetier, D., Oyallon, J., Morin-Poulard, I., Dejean, S., Vincent, A., and Crozatier, M. (2012). Size control of the Drosophila hematopoietic niche by bone morphogenetic protein signaling reveals parallels with mammals. Proc. Natl. Acad. Sci. USA *109*, 3389–3394. https://doi.org/10.1073/pnas.1109407109.

21. Austin, T.W., Solar, G.P., Ziegler, F.C., Liem, L., and Matthews, W. (1997). A Role for the Wnt Gene Family in Hematopoiesis: Expansion of Multilineage Progenitor Cells. Blood *89*, 3624–3635. https://doi.org/10.1182/blood.V89.10.3624.

22. Sinenko, S.A., Mandal, L., Martinez-Agosto, J.A., and Banerjee, U. (2009). Dual role of Wingless signaling in stem-like hematopoietic precursor maintenance in Drosophila. Dev. Cell *16*, 756–763. https://doi.org/10.1016/j.devcel.2009.03.003.

23. Morin-Poulard, I., Sharma, A., Louradour, I., Vanzo, N., Vincent, A., and Crozatier, M. (2016). Vascular control of the Drosophila haematopoietic microenvironment by Slit/Robo signalling. Nat. Commun. *7*, 11634. https://doi.org/10.1038/ncomms11634.

24. Benmimoun, B., Polesello, C., Haenlin, M., and Waltzer, L. (2015). The EBF transcription factor Collier directly promotes Drosophila blood cell progenitor maintenance independently of the niche. Proc. Natl. Acad. Sci. USA *112*, 9052–9057. https://doi.org/10.1073/pnas.1423967112.

25. Kieslinger, M., Hiechinger, S., Dobreva, G., Consalez, G.G., and Grosschedl, R. (2010). Early B Cell Factor 2 Regulates Hematopoietic Stem Cell Homeostasis in a Cell-Nonautonomous Manner. Cell Stem Cell *7*, 496–507. https://doi.org/10.1016/j.stem.2010.07.015.

26. Bazzi, W., Cattenoz, P.B., Delaporte, C., Dasari, V., Sakr, R., Yuasa, Y., and Giangrande, A. (2018). Embryonic hematopoiesis modulates the inflammatory response and larval hematopoiesis in Drosophila. eLife *7*, e34890. https://doi.org/10.7554/eLife.34890.

27. Lanot, R., Zachary, D., Holder, F., and Meister, M. (2001). Postembryonic Hematopoiesis in Drosophila. Dev. Biol. *230*, 243–257. https://doi.org/10.1006/dbio.2000.0123.

28. Grigorian, M., Mandal, L., and Hartenstein, V. (2011). Hematopoiesis at the onset of metamorphosis: terminal differentiation and dissociation of the Drosophila lymph gland. Dev. Genes Evol. *221*, 121–131. https://doi.org/10.1007/s00427-011-0364-6.

29. Charroux, B., and Royet, J. (2009). Elimination of plasmatocytes by targeted apoptosis reveals their role in multiple aspects of the Drosophila immune response. Proc. Natl. Acad. Sci. US A *106*, 9797–9802. https://doi.org/10.1073/pnas.0903971106.

30. Shia, A.K.H., Glittenberg, M., Thompson, G., Weber, A.N., Reichhart, J.-M., and Ligoxygakis, P. (2009). Toll-dependent antimicrobial responses in Drosophila larval fat body require Spätzle secreted by haemocytes. J. Cell Sci. *122*, 4505–4515. https://doi.org/10.1242/jcs.049155.

31. Arefin, B., Kucerova, L., Krautz, R., Kranenburg, H., Parvin, F., and Theopold, U. (2015). Apoptosis in Hemocytes Induces a Shift in Effector Mechanisms in the Drosophila Immune System and Leads to a Pro-Inflammatory State. PLOS ONE *10*, e0136593. https://doi.org/10.1371/journal.pone.0136593.

32. Tomar, A., Madhwal, S., and Mukherjee, T. (2020). Immune Control of Animal Growth in Homeostasis and Nutritional Stress in Drosophila. Front. Immunol. *11*, 1528. https://doi.org/10.3389/fimmu.2020.01528.

33. Shin, M., Cha, N., Koranteng, F., Cho, B., and Shim, J. (2020). Subpopulation of Macrophage-Like Plasmatocytes Attenuates Systemic Growth via JAK/STAT in the Drosophila Fat Body. Front. Immunol. *11*, 63. https://doi.org/10.3389/fimmu.2020.00063.

34. Grether, M.E., Abrams, J.M., Agapite, J., White, K., and Steller, H. (1995). The head involution defective gene of Drosophila melanogaster functions in programmed cell death. Genes Dev. *9*, 1694–1708. https://doi.org/10.1101/gad.9.14.1694.

35. Sinenko, S.A., and Mathey-Prevot, B. (2004). Increased expression of Drosophila tetraspanin, Tsp68C, suppresses the abnormal proliferation of ytr-deficient and Ras/Raf-activated hemocytes. Oncogene *23*, 9120–9128. https://doi.org/10.1038/sj.onc.1208156.

36. Goto, A., Kadowaki, T., and Kitagawa, Y. (2003). Drosophila hemolectin gene is expressed in embryonic and larval hemocytes and its knock down causes bleeding defects. Dev. Biol. *264*, 582–591. https://doi.org/10.1016/j.ydbio.2003.06.001.

37. Defaye, A., Evans, I., Crozatier, M., Wood, W., Lemaitre, B., and Leulier, F. (2009). Genetic Ablation of *Drosophila* Phagocytes Reveals Their Contribution to Both Development and Resistance to Bacterial Infection. J. Innate Immun. *1*, 322–334. https://doi.org/10.1159/000210264.

38. Jung, S.H., Evans, C.J., Uemura, C., and Banerjee, U. (2005). The Drosophila lymph gland as a developmental model of hematopoiesis. Development *132*, 2521–2533. https://doi.org/10.1242/dev.01837.

39. Mondal, B.C., Mukherjee, T., Mandal, L., Evans, C.J., Sinenko, S.A., Martinez-Agosto, J.A., and Banerjee, U. (2011). Interaction between Differentiating Cell- and Niche-Derived Signals in Hematopoietic Progenitor Maintenance. Cell *147*, 1589–1600. https://doi.org/10.1016/j.cell.2011.11.041.

40. Honti, V., Kurucz, E., Csordás, G., Laurinyecz, B., Márkus, R., and Andó, I. (2009). In vivo detection of lamellocytes in Drosophila melanogaster. Immunol. Lett. *126*, 83–84. https://doi.org/10.1016/j.imlet.2009.08.004.

41. Irving, P., Ubeda, J.M., Doucet, D., Troxler, L., Lagueux, M., Zachary, D., Hoffmann, J.A., Hetru, C., and Meister, M. (2005). New insights into Drosophila larval haemocyte functions through genome-wide analysis. Cell. Microbiol. *7*, 335–350. https://doi.org/10.1111/j.1462-5822.2004.00462.x.

42. Song, Z., McCall, K., and Steller, H. (1997). DCP-1, a Drosophila Cell Death Protease Essential for Development. Science *275*, 536–540. https://doi.org/10.1126/science.275.5299.536.

43. Nelson, R.E., Fessler, L.I., Takagi, Y., Blumberg, B., Keene, D.R., Olson, P.F., Parker, C.G., and Fessler, J.H. (1994). Peroxidasin: a novel enzyme-matrix protein of Drosophila development. EMBO J. *13*, 3438–3447. https://doi.org/10.1002/j.1460-2075.1994.tb06649.x.

44. Kurucz, E., Zettervall, C.-J., Sinka, R., Vilmos, P., Pivarcsi, A., Ekengren, S., Hegedüs, Z., Ando, I., and Hultmark, D. (2003). Hemese, a hemocyte-specific transmembrane protein, affects the cellular immune response in Drosophila. Proc. Natl. Acad. Sci. USA *100*, 2622–2627. https://doi.org/10.1073/pnas.0436940100.

45. Kocks, C., Cho, J.H., Nehme, N., Ulvila, J., Pearson, A.M., Meister, M., Strom, C., Conto, S.L., Hetru, C., Stuart, L.M., et al. (2005). Eater, a Transmembrane Protein Mediating Phagocytosis of Bacterial Pathogens in Drosophila. Cell *123*, 335–346. https://doi.org/10.1016/j.cell.2005.08.034.

46. Kurucz, E., Márkus, R., Zsámboki, J., Folkl-Medzihradszky, K., Darula, Z., Vilmos, P., Udvardy, A., Krausz, I., Lukacsovich, T., Gateff, E., et al. (2007). Nimrod, a Putative Phagocytosis Receptor with EGF Repeats in

Drosophila Plasmatocytes. Curr. Biol. *17*, 649–654. https://doi.org/10.1016/j.cub.2007.02.041.

47. Pérez-Cadahía, B., Drobic, B., and Davie, J.R. (2009). H3 phosphorylation: dual role in mitosis and interphase. Biochem. Cell Biol. *87*, 695–709. https://doi.org/10.1139/O09-053.
48. Pérez-Garijo, A., Fuchs, Y., and Steller, H. (2013). Apoptotic cells can induce non-autonomous apoptosis through the TNF pathway. eLife *2*, e01004. https://doi.org/10.7554/eLife.01004.
49. Agaisse, H., Petersen, U.M., Boutros, M., Mathey-Prevot, B., and Perrimon, N. (2003). Signaling Role of Hemocytes in Drosophila JAK/STAT-Dependent Response to Septic Injury. Dev. Cell *5*, 441–450. https://doi.org/10.1016/S1534-5807(03)00244-2.
50. Yang, H., Kronhamn, J., Ekström, J.-O., Korkut, G.G., and Hultmark, D. (2015). JAK/STAT signaling in Drosophila muscles controls the cellular immune response against parasitoid infection. EMBO Rep. *16*, 1664–1672. https://doi.org/10.15252/embr.201540277.
51. Elsaid, R., Soares-da-Silva, F., Peixoto, M., Amiri, D., Mackowski, N., Pereira, P., Bandeira, A., and Cumano, A. (2020). Hematopoiesis: A Layered Organization Across Chordate Species. Front. Cell Dev. Biol. *8*, 606642. https://doi.org/10.3389/fcell.2020.606642.
52. Spangenberg, E., Severson, P.L., Hohsfield, L.A., Crapser, J., Zhang, J., Burton, E.A., Zhang, Y., Spevak, W., Lin, J., Phan, N.Y., et al. (2019). Sustained microglial depletion with CSF1R inhibitor impairs parenchymal plaque development in an Alzheimer's disease model. Nat. Commun. *10*, 3758. https://doi.org/10.1038/s41467-019-11674-z.
53. Elmore, M.R.P., Najafi, A.R., Koike, M.A., Dagher, N.N., Spangenberg, E.E., Rice, R.A., Kitazawa, M., Matusow, B., Nguyen, H., West, B.L., and Green, K.N. (2014). Colony-Stimulating Factor 1 Receptor Signaling Is Necessary for Microglia Viability, Unmasking a Microglia Progenitor Cell in the Adult Brain. Neuron *82*, 380–397. https://doi.org/10.1016/j.neuron.2014.02.040.
54. Gentek, R., Ghigo, C., Hoeffel, G., Bulle, M.J., Msallam, R., Gautier, G., Launay, P., Chen, J., Ginhoux, F., and Bajénoff, M. (2018). Hemogenic Endothelial Fate Mapping Reveals Dual Developmental Origin of Mast Cells. Immunity *48*, 1160–1171.e5. https://doi.org/10.1016/j.immuni.2018.04.025.
55. De, S., Van Deren, D., Peden, E., Hockin, M., Boulet, A., Titen, S., and Capecchi, M.R. (2018). Two distinct ontogenies confer heterogeneity to mouse brain microglia. Development *145*, dev152306. https://doi.org/10.1242/dev.152306.
56. Kiel, M.J., Yilmaz, O.H., Iwashita, T., Yilmaz, O.H., Terhorst, C., and Morrison, S.J. (2005). SLAM Family Receptors Distinguish Hematopoietic Stem and Progenitor Cells and Reveal Endothelial Niches for Stem Cells. Cell *121*, 1109–1121. https://doi.org/10.1016/j.cell.2005.05.026.
57. Edgar, B.A., and O'Farrell, P.H. (1989). Genetic control of cell division patterns in the Drosophila embryo. Cell *57*, 177–187. https://doi.org/10.1016/0092-8674(89)90183-9.
58. Neves, A., and Eisenman, R.N. (2019). Distinct gene-selective roles for a network of core promoter factors in Drosophila neural stem cell identity. Biol. Open *8*, bio042168. https://doi.org/10.1242/bio.042168.
59. Okuda, K., Tong, M., Dempsey, B., Moore, K.J., Gazzinelli, R.T., and Silverman, N. (2016). Leishmania amazonensis Engages CD36 to Drive Parasitophorous Vacuole Maturation. PLOS Pathog. *12*, e1005669. https://doi.org/10.1371/journal.ppat.1005669.
60. Grigorian, M., Liu, T., Banerjee, U., and Hartenstein, V. (2013). The proteoglycan Trol controls the architecture of the extracellular matrix and balances proliferation and differentiation of blood progenitors in the Drosophila lymph gland. Dev. Biol. *384*, 301–312. https://doi.org/10.1016/j.ydbio.2013.03.007.
61. Matsubayashi, Y., Louani, A., Dragu, A., Sánchez-Sánchez, B.J., Serna-Morales, E., Yolland, L., Gyoergy, A., Vizcay, G., Fleck, R.A., Heddleston, J.M., et al. (2017). A Moving Source of Matrix Components Is Essential for De Novo Basement Membrane Formation. Curr. Biol. *27*, 3526–3534.e4. https://doi.org/10.1016/j.cub.2017.10.001.
62. Cattenoz, P.B., Sakr, R., Pavlidaki, A., Delaporte, C., Riba, A., Molina, N., Hariharan, N., Mukherjee, T., and Giangrande, A. (2020). Temporal specificity and heterogeneity of Drosophila immune cells. EMBO J. *39*, e104486. https://doi.org/10.15252/embj.2020104486.
63. Lindner, J.R., Hillman, P.R., Barrett, A.L., Jackson, M.C., Perry, T.L., Park, Y., and Datta, S. (2007). The Drosophila Perlecan gene trol regulates multiple signaling pathways in different developmental contexts. BMC Dev. Biol. *7*, 121. https://doi.org/10.1186/1471-213X-7-121.
64. Fessler, J.H., and Fessler, L.I. (1989). Drosophila Extracellular Matrix. Annu. Rev. Cell. Biol. *5*, 309–339. https://doi.org/10.1146/annurev.cb.05.110189.001521.
65. Yasothornsrikul, S., Davis, W.J., Cramer, G., Kimbrell, D.A., and Dearolf, C.R. (1997). viking: identification and characterization of a second type IV collagen in Drosophila. Gene *198*, 17–25. https://doi.org/10.1016/S0378-1119(97)00274-6.
66. Kusche-Gullberg, M., Garrison, K., MacKrell, A.J., Fessler, L.I., and Fessler, J.H. (1992). Laminin A chain: expression during Drosophila development and genomic sequence. EMBO J. *11*, 4519–4527. https://doi.org/10.1002/j.1460-2075.1992.tb05553.x.
67. Martinek, N., Zou, R., Berg, M., Sodek, J., and Ringuette, M. (2002). Evolutionary conservation and association of SPARC with the basal lamina in Drosophila. Dev. Genes Evol. *212*, 124–133. https://doi.org/10.1007/s00427-002-0220-9.
68. Brand, A.H., and Perrimon, N. (1993). Targeted gene expression as a means of altering cell fates and generating dominant phenotypes. Development *118*, 401–415. https://doi.org/10.1242/dev.118.2.401.
69. Gao, H., Wu, X., and Fossett, N. (2013). Drosophila E-Cadherin Functions in Hematopoietic Progenitors to Maintain Multipotency and Block Differentiation. PLOS ONE *8*, e74684. https://doi.org/10.1371/journal.pone.0074684.
70. Evans, C.J., Liu, T., and Banerjee, U. (2014). Drosophila hematopoiesis: Markers and methods for molecular genetic analysis. Methods *68*, 242–251. https://doi.org/10.1016/j.ymeth.2014.02.038.
71. Khadilkar, R.J., Ho, K.Y.L., Venkatesh, B., and Tanentzapf, G. (2020). Integrins Modulate Extracellular Matrix Organization to Control Cell Signaling during Hematopoiesis. Curr. Biol. *30*, 3316–3329.e5. https://doi.org/10.1016/j.cub.2020.06.027.
72. Shiojiri, N., and Sugiyama, Y. (2004). Immunolocalization of extracellular matrix components and integrins during mouse liver development. Hepatology *40*, 346–355. https://doi.org/10.1002/hep.20303.
73. Mahony, C.B., and Bertrand, J.Y. (2019). How HSCs Colonize and Expand in the Fetal Niche of the Vertebrate Embryo: An Evolutionary Perspective. Front. Cell Dev. Biol. *7*, 34. https://doi.org/10.3389/fcell.2019.00034.
74. Ajami, B., Bennett, J.L., Krieger, C., McNagny, K.M., and Rossi, F.M.V. (2011). Infiltrating monocytes trigger EAE progression, but do not contribute to the resident microglia pool. Nat. Neurosci. *14*, 1142–1149. https://doi.org/10.1038/nn.2887.
75. Misharin, A.V., Morales-Nebreda, L., Reyfman, P.A., Cuda, C.M., Walter, J.M., McQuattie-Pimentel, A.C., Chen, C.-I., Anekalla, K.R., Joshi, N., Williams, K.J.N., et al. (2017). Monocyte-derived alveolar macrophages drive lung fibrosis and persist in the lung over the life span. J. Exp. Med. *214*, 2387–2404. https://doi.org/10.1084/jem.20162152.
76. Bajpai, G., Bredemeyer, A., Li, W., Zaitsev, K., Koenig, A.L., Lokshina, I., Mohan, J., Ivey, B., Hsiao, H.-M., Weinheimer, C., et al. (2019). Tissue Resident CCR2− and CCR2+ Cardiac Macrophages Differentially Orchestrate Monocyte Recruitment and Fate Specification Following Myocardial Injury. Circ. Res. *124*, 263–278. https://doi.org/10.1161/CIRCRESAHA.118.314028.
77. Shechter, R., London, A., Varol, C., Raposo, C., Cusimano, M., Yovel, G., Rolls, A., Mack, M., Pluchino, S., Martino, G., et al. (2009). Infiltrating Blood-Derived Macrophages Are Vital Cells Playing an Anti-inflammatory Role in Recovery from Spinal Cord Injury in Mice. PLOS Med. *6*, e1000113. https://doi.org/10.1371/journal.pmed.1000113.

78. Duffield, J.S., Forbes, S.J., Constandinou, C.M., Clay, S., Partolina, M., Vuthoori, S., Wu, S., Lang, R., and Iredale, J.P. (2005). Selective depletion of macrophages reveals distinct, opposing roles during liver injury and repair. J. Clin. Invest. *115*, 56–65. https://doi.org/10.1172/JCI22675.

79. Weinberger, T., Esfandyari, D., Messerer, D., Percin, G., Schleifer, C., Thaler, R., Liu, L., Stremmel, C., Schneider, V., Vagnozzi, R.J., et al. (2020). Ontogeny of arterial macrophages defines their functions in homeostasis and inflammation. Nat. Commun. *11*, 4549. https://doi.org/10.1038/s41467-020-18287-x.

80. Blériot, C., Dupuis, T., Jouvion, G., Eberl, G., Disson, O., and Lecuit, M. (2015). Liver-Resident Macrophage Necroptosis Orchestrates Type 1 Microbicidal Inflammation and Type-2-Mediated Tissue Repair during Bacterial infection. Immunity *42*, 145–158. https://doi.org/10.1016/j.immuni.2014.12.020.

81. Wang, T., Zhang, J., Wang, Y., Li, Y., Wang, L., Yu, Y., and Yao, Y. (2023). Influenza-trained mucosal-resident alveolar macrophages confer long-term antitumor immunity in the lungs. Nat. Immunol. *24*, 423–438. https://doi.org/10.1038/s41590-023-01428-x.

82. Madsen, D.H., Jürgensen, H.J., Siersbæk, M.S., Kuczek, D.E., Grey Cloud, L.G., Liu, S., Behrendt, N., Grøntved, L., Weigert, R., and Bugge, T.H. (2017). Tumor-Associated Macrophages Derived from Circulating Inflammatory Monocytes Degrade Collagen through Cellular Uptake. Cell Rep. *21*, 3662–3671. https://doi.org/10.1016/j.celrep.2017.12.011.

83. Zhu, Y., Herndon, J.M., Sojka, D.K., Kim, K.-W., Knolhoff, B.L., Zuo, C., Cullinan, D.R., Luo, J., Bearden, A.R., Lavine, K.J., et al. (2017). Tissue-Resident Macrophages in Pancreatic Ductal Adenocarcinoma Originate from Embryonic Hematopoiesis and Promote Tumor Progression. Immunity *47*, 323–338.e6. https://doi.org/10.1016/j.immuni.2017.07.014.

84. Hutter, G., Theruvath, J., Graef, C.M., Zhang, M., Schoen, M.K., Manz, E.M., Bennett, M.L., Olson, A., Azad, T.D., Sinha, R., et al. (2019). Microglia are effector cells of CD47-SIRPα antiphagocytic axis disruption against glioblastoma. Proc. Natl. Acad. Sci. USA *116*, 997–1006. https://doi.org/10.1073/pnas.1721434116.

85. Loyher, P.L., Hamon, P., Laviron, M., Meghraoui-Kheddar, A., Goncalves, E., Deng, Z., Torstensson, S., Bercovici, N., Baudesson de Chanville, C., Combadière, B., et al. (2018). Macrophages of distinct origins contribute to tumor development in the lung. J. Exp. Med. *215*, 2536–2553. https://doi.org/10.1084/jem.20180534.

86. Destalminil-Letourneau, M., Morin-Poulard, I., Tian, Y., Vanzo, N., and Crozatier, M. (2021). The vascular niche controls Drosophila hematopoiesis via fibroblast growth factor signaling. eLife *10*, e64672. https://doi.org/10.7554/eLife.64672.

87. Shim, J., Mukherjee, T., and Banerjee, U. (2012). Direct sensing of systemic and nutritional signals by haematopoietic progenitors in Drosophila. Nat. Cell Biol. *14*, 394–400. https://doi.org/10.1038/ncb2453.

88. Shim, J., Mukherjee, T., Mondal, B.C., Liu, T., Young, G.C., Wijewarnasuriya, D.P., and Banerjee, U. (2013). Olfactory control of blood progenitor maintenance. Cell *155*, 1141–1153. https://doi.org/10.1016/j.cell.2013.10.032.

89. Cho, B., Spratford, C.M., Yoon, S., Cha, N., Banerjee, U., and Shim, J. (2018). Systemic control of immune cell development by integrated carbon dioxide and hypoxia chemosensation in Drosophila. Nat. Commun. *9*, 2679. https://doi.org/10.1038/s41467-018-04990-3.

90. Travnickova, J., Tran Chau, V., Julien, E., Mateos-Langerak, J., Gonzalez, C., Lelièvre, E., Lutfalla, G., Tavian, M., and Kissa, K. (2015). Primitive macrophages control HSPC mobilization and definitive haematopoiesis. Nat. Commun. *6*, 6227. https://doi.org/10.1038/ncomms7227.

91. Mass, E., Ballesteros, I., Farlik, M., Halbritter, F., Günther, P., Crozet, L., Jacome-Galarza, C.E., Händler, K., Klughammer, J., Kobayashi, Y., et al. (2016). Specification of tissue-resident macrophages during organogenesis. Science *353*, aaf4238. https://doi.org/10.1126/science.aaf4238.

92. Han, X., Wang, R., Zhou, Y., Fei, L., Sun, H., Lai, S., Saadatpour, A., Zhou, Z., Chen, H., Ye, F., et al. (2018). Mapping the Mouse Cell Atlas by Microwell-Seq. Cell *172*, 1091–1107.e17. https://doi.org/10.1016/j.cell.2018.02.001.

93. Yoon, S., Cho, B., Shin, M., Koranteng, F., Cha, N., and Shim, J. (2017). Iron Homeostasis Controls Myeloid Blood Cell Differentiation in Drosophila. Mol. Cells *40*, 976–985. https://doi.org/10.14348/molcells.2017.0287.

94. Kurucz, E., Váczi, B., Márkus, R., Laurinyecz, B., Vilmos, P., Zsámboki, J., Csorba, K., Gateff, E., Hultmark, D., and Andó, I. (2007). Definition of Drosophila hemocyte subsets by cell-type specific antigens. Acta Biol. Hung. *58* (suppl), 95–111. https://doi.org/10.1556/ABiol.58.2007.Suppl.8.

95. Díaz-Torres, A., Rosales-Nieves, A.E., Pearson, J.R., Santa-Cruz Mateos, C., Marín-Menguiano, M., Marshall, O.J., Brand, A.H., and González-Reyes, A. (2021). Stem cell niche organization in the Drosophila ovary requires the ECM component Perlecan. Curr. Biol. *31*, 1744–1753.e5. https://doi.org/10.1016/j.cub.2021.01.071.

96. Van De Bor, V., Zimniak, G., Papone, L., Cerezo, D., Malbouyres, M., Juan, T., Ruggiero, F., and Noselli, S. (2015). Companion Blood Cells Control Ovarian Stem Cell Niche Microenvironment and Homeostasis. Cell Rep. *13*, 546–560. https://doi.org/10.1016/j.celrep.2015.09.008.

97. Schindelin, J., Arganda-Carreras, I., Frise, E., Kaynig, V., Longair, M., Pietzsch, T., Preibisch, S., Rueden, C., Saalfeld, S., Schmid, B., et al. (2012). Fiji: an open-source platform for biological-image analysis. Nat. Methods *9*, 676–682. https://doi.org/10.1038/nmeth.2019.

98. Peixoto, M.M., Soares-da-Silva, F., Bonnet, V., Ronteix, G., Santos, R.F., Mailhe, M.-P., Feng, X., Pereira, J.P., Azzoni, E., Anselmi, G., et al. (2023). Spatiotemporal dynamics of cytokines expression dictate fetal liver hematopoiesis. Preprint at bioRxiv. https://doi.org/10.1101/2023.08.24.554612.

STAR★METHODS

KEY RESOURCES TABLE

REAGENT or RESOURCE	SOURCE	IDENTIFIER
Antibodies		
chicken anti-GFP	abcam	Cat# 13970; RRID: AB_300798
rabbit anti-Peroxidasin	gift from Jiwon Shim, Hanyang University (Yoon et al.[93])	N/A
mouse anti-Hemese	gift from István Andó, HUN Biological Research Centre (Kurucz et al.[44])	N/A
mouse anti-PH3	Millipore	Cat# 05-806; RRID: AB_310016
rabbit ati-Dcp1	Cell signaling	Cat# 9578; RRID: AB_2721060
mouse anti-Atilla	gift from István Andó, HUN Biological Research Centre (Kurucz et al.[94])	N/A
mouse anti-L4	gift from István Andó, HUN Biological Research Centre (Kurucz et al.[94])	N/A
rabbit anti trol	gift from Acaimo González-Reyes, CSIC/Universidad Pablo de Olavide/JA (Díaz-Torres et al.[95])	N/A
rabbit anti Cg25c	gift from Stéphane Noselli, University of Nice Sophia Antipolis, Institut de Biologie Valrose (Van De Bor et al.[96])	N/A
mouse anti-Antp	DSHB	Cat# anti-Antp 4C3; RRID: AB_528082
mouse anti-Antp	DSHB	Cat# anti-Antp 8C11; RRID: AB_528083
Rat anti-E-Cadherin	DSHB	Cat# DCAD2; RRID: AB_528120
mouse anti-βPS integrin	DSHB	Cat# cf.6g11; RRID: AB_528310
mouse anti-Wg	DSHB	Cat# 4d4; RRID: AB_528512
donkey anti-chicken FITC	Jackson ImmunoResearch	Cat# 703-095-155; RRID: AB_2340356
goat anti-mouse Alexa Fluor 647	Jackson ImmunoResearch	Cat# 115-605-166; RRID: AB_2338914
donkey anti-rabbit Cy3	Jackson ImmunoResearch	Cat# 711-165-152; RRID: AB_2307443
CD16/32 BUV737 (Clone 2.4G2)	BD Biosciences	Cat# 612783; RRID:AB_2870112
CD16/32 BV711 (Clone 2.4G2)	Biolegend	Cat# 101337; RRID:AB_2565637
CD16/32 Fc Block™ (Clone 2.4G2)	BD Biosciences	Cat# 553142; RRID:AB_394657
CD45 BUV395 (Clone 30-F11)	BD Biosciences	Cat# 564279; RRID:AB_2651134
CD45 BV510 (Clone 30-F11)	BD Biosciences	Cat# 563891 ; RRID:AB_2734134
CD45 FITC (Clone 30-F11)	BD Biosciences	Cat# 553080 ; RRID:AB_394610
F4/80 BV785 (Clone BM8)	Biolegend	Cat# 123141; RRID:AB_2563667
F4/80 BV421 (Clone BM8)	Sony Biotechnology Inc.	Cat# 1215660; RRID: AB_11203717
F4/80 biotin (Clone BM8)	Biolegend	Cat# 123106; RRID:AB_893501
Ly-6G BV711 (Clone 1A8)	BD Biosciences	Cat# 563979; RRID:AB_2738520
Ly-6G BV421 (Clone 1A8)	BD Biosciences	Cat# 562737; RRID:AB_2737756
Ly-6C BV510 (Clone HK1.4)	Biolegend	Cat# 128033 ; RRID:AB_2562351
Ly-6C eF450 (Clone HK1.4)	eBioscience	Cat# 15321810
Sca-1 BV711 (Clone D7)	Biolegend	Cat# 108131; RRID:AB_2562241
Sac-1 BV510 (Clone D7)	Biolegend	Cat# 108129; RRID:AB_2561593
CD34 eF450 (Clone RAM34)	eBioscience	Cat# 48-0341-82; RRID:AB_2043837

(*Continued on next page*)

Continued

REAGENT or RESOURCE	SOURCE	IDENTIFIER
CD34 eF660 (Clone RAM34)	eBioscience	Cat# 50-0341-80; RRID:AB_10609352
Ter119 BV785 (Clone TER-119)	Biolegend	Cat# 116245; RRID:AB_2650921
Ter119 biotin (Clone TER-119)	Biolegend	Cat# 116204; RRID:AB_313705
CD19 biotin (Clone 1D3)	BD Biosciences	Cat# 553784; RRID:AB_395048
CD3e biotin (Clone 145-2C11)	BD Biosciences	Cat# 553060; RRID:AB_394593
Gr1 biotin (Clone RB6-8C5)	BD Biosciences	Cat# 553124; RRID:AB_394640
NK1.1 biotin (Clone PK136)	Biolegend	Cat# 108704; RRID:AB_313391
CD115 FITC (Clone AFS98)	TONBObiosciences	Cat# TNB35-1152-U025
CD115 PE (Clone AFS98)	eBioscience	Cat# 12-1152-83; RRID:AB_465809
CD115 PE-CF594 (Clone AFS98)	Biolegend	Cat# 135527; RRID:AB_2566522
CD115 APC (Clone AFS98)	eBioscience	Cat# 17-1152-82; RRID:AB_1210789
Flt3 PE-CF594 (Clone A2F10)	BD Biosciences	Cat# 562537 ; RRID:AB_2737639
Kit BV711 (Clone 2B8)	BD Biosciences	Cat# 563160; RRID:AB_2722510
Kit PE (Clone 2B8)	BD Biosciences	Cat# 553355; RRID:AB_394806
Kit APC-Cy7 (Clone 2B8)	Sony Biotechnology Inc.	Cat# 1129130; RRID: AB_1626278
CD11b PE (Clone M1/70)	Biolegend	Cat# 101208; RRID:AB_312791
CD11b PE-Cy7 (Clone M1/70)	BD Biosciences	Cat# 552850; RRID:AB_394491
CD11b BB515 (Clone M1/70)	BD Biosciences	Cat# 564454; RRID:AB_2665392
CD11b APC-Cy7 (Clone M1/70)	BD Biosciences	Cat# 557657; RRID:AB_396772
CD11b AF700 (Clone M1/70)	BD Biosciences	Cat# 557960; RRID:AB_396960
CD150 PE-Cy7 (Clone mShad150)	eBioscience	Cat# 25-1502-80; RRID:AB_10804766
CD48 BUV395 (Clone HM48-1)	BD Biosciences	Cat# 740236; RRID:AB_2739984
CD64 BV711 (Clone X54-5/7.1)	Biolegend	Cat# 139311 ; RRID:AB_2563846
CD64 PE-Cy7 (Clone X54-5/7.1)	Sony Biotechnology Inc.	Cat# 1296570; RRID:AB_2917921
CD64 APC (Clone X54-5/7.1)	Biolegend	Cat# 139306; RRID:AB_11219391
CD41 BUV395 (Clone MWReg30)	BD Biosciences	Cat# 752966; RRID: AB_2917921
Tim4 BUV737 (Clone RMT4-54)	BD Biosciences	Cat# 749134; RRID:AB_2873523
Tim4 PE-Cy7 (Clone RMT4-54)	Biolegend	Cat# 130010; RRID:AB_2565719
IL33Ra (ST2) PE/Dazzle (Clone DIH9)	Biolegend	Cat# 145314; RRID:AB_2687364
Ki67 AlexaFluor647 (Clone B56)	BD Biosciences	Cat# 558615; RRID:AB_647130
Streptavidin BUV737	BD Biosciences	Cat# 564293; RRID: AB_2869560
Streptavidin BV785	Biolegend	Cat# 405249
rat anti-mouse CD68	Biorad	Cat# MCA1957; RRID:AB_322219
rabbit anti-mouse Collagen IV	Biorad	Cat# 2150-1470; RRID:AB_2082660
goat anti-rat AF555	Invitrogen	Cat# A-21434; RRID:AB_1417833
goat anti-rabbit AF555	Invitrogen	Cat# A-21429; RRID:AB_2535850
Chemicals, peptides, and recombinant proteins		
N-Phenylthiourea	Sigma-Aldrich	P7629
PFA	Electron Microscopy Sciences	50-980-487
NGS	Vector Laboratories	Cat# S-10000
DAPI	Sigma-Aldrich	Cat# D9542
Vectashield	Vector Laboratories	H-1000-10
TRI-reagent	Molecular Research Center	TR 118
AIN-76A Rodent Diet With 1,200 mg PLX5622 (Free Base)/kg	Research Diets, Inc.	Cat# D11100404i; Lot: 21121410A5HSi
4-Hydroxytamoxifen	Sigma	Cat# H7904-25MG
Kolliphor EL	Sigma	Cat# C5135-500G
Progesterone	Sigma	Cat# P3972-5G
Sunflower oil	Sigma	Cat# S5007-250ML

(*Continued on next page*)

Continued

REAGENT or RESOURCE	SOURCE	IDENTIFIER
0.5M EDTA pH 8.0	Invitrogen	Cat# AM9260G
Collagenase D	Sigma	Cat# 11088882001
DNase I	Sigma	Cat# DN25-100MG
Dispase II	Invitrogen	Cat# 17105-041
Liberase DL	Roche	Cat# 5466202001
Collagenase I	Gibco	Cat# 17018029
ChromPure Mouse IgG	Jackson ImmunoResearch	Cat# 015-000-003; RRID:AB_2337188
Sytox™ Green dead cell stain	Invitrogen	Cat# S34860
RNAprotect	Qiagen	Cat# 76104
Stainless steel bead	Qiagen	Cat# 69989
Tissue Lyser II	Qiagen	Cat# 85300
Formalin solution, neutral buffered, 10%	Sigma	Cat# HT5014-1CS
O.C.T™	Tissue-Tek®	Cat# 4583
Dapi (mouse experiments)	Invitrogen	Cat# 10116287
NGS (mouse experiments)	Gibco	Cat# 16210064
RapiClear® 1.52	SUNJin Lab	Cat# RC152001
ProLong™ Gold Antifade Mounting	Invitrogen	Cat# P36930
Stem Cell Factor (Kit ligand)	N/A	N/A
Mouse Granulocyte Macrophage Colony Stimulating Factor (mGM-CSF)	Cell Signaling Technology	Cat# 70343
Mouse Macrophage Colony Stimulating Factor (mM-CSF)	Cell Signaling Technology	Cat# 33444
rmEpo (Recombinant Mouse Erythropoietin)	R&D Systems	Cat# 959-ME-010
rmTpo (Recombinant Mouse Thrombopoietin)	R&D Systems	Cat# 488-TO-025
OptiMEM-I W/Glutamax	Gibco	51985026
2-Mercaptoethanol	Gibco	31350010
Penicillin Streptomycin Solution	Gibco	15070063
Critical commercial assays		
DNase I recombinant RNase free	Roche	Cat# 04716728001
Super-Script IV	Invitrogen	Cat# 18091050
SYBR Green I Master Mix	Roche	Cat# 04673492001
RNeasy Plus Mini Kit	Qiagen	Cat# 74134
PrimeScript™ RT Reagent Kit	Takara	Cat# RR037A
TaqMan™ Fast Advanced Master Mix	Applied Biosystems™	Cat# 12634225
Mouse Immune array	Applied Biosystems™	Cat# 4418724
Customized mouse Extracellular Matrix and Adhesion molecules plates	Applied Biosystems™	N/A
BD Cytofix/Cytoperm™	BD Biosciences	Cat# 554714
In Situ Cell Death Detection Kit, TMR red	Roche	Cat# 12156792910
Anti-Biotin MicroBeads	Miltenyi Biotec	Cat# 130-090-485
MS columns	Miltenyi Biotec	Cat# 130-042-201
Experimental models: Organisms/strains		
Fly: *w^{1118}*	BDSC	5905
Fly: *HmlΔGal4, UAS-2XEGFP*	BDSC	30140
Fly: *HmlΔGal4*	BDSC	30139
Fly: *UAS-hid*	BDSC	65403
Fly: *stg* RNAi	BDSC	36094
Fly: *eater RNAi*	BDSC	25863
Fly: *trol RNAi*	BDSC	29440

(*Continued on next page*)

Continued

REAGENT or RESOURCE	SOURCE	IDENTIFIER
Fly: *vkg RNAi*	BDSC	50895
Fly: *UAS-trol*	BDSC	65273
Fly: *UbiGal4*	BDSC	32551
Fly: *domeMeso-EBFP2*	gift from Jiwon Shim, Hanyang University (Evans et al.[70])	N/A
Mouse: *Cdh5^{CreERT2}*	Gift from Ralf H Adams, Max Planck Institute for Molecular Biomedicine.	MGI:3848982
Mouse: *Rosa26^{tdTomato}*	Institut Pasteur animal facility	MGI:3809524
Mouse: C57BL/6JRj	Janvier	RRID:IMSR_RJ:C57BL-6JRJ
Oligonucleotides		
Act5C (F) GCAAGAGGATCAGGATCGGG *(R)* TGCTGCACTCCAAACTTCCA	Sigma-Aldrich	N/A
Rp49 (F) GACGCTTCAAGGGACAGTA *(R)* AAACGCGGTTCTGCATGAG	Sigma-Aldrich	N/A
Hml (F) AATCGAGAGCACCCGGAAAG *(R)* GCCACAACTGATGGGACAGA	Sigma-Aldrich	N/A
Pxn (F) AACTGCCCCAGGATACACAAA *(R)* TAAGCCAGCTCGTTGTCGTT	Sigma-Aldrich	N/A
Eater (F) ATGGCTGTAGCAACGGAGTTT *(R)* CTTGCAAACAGGAGTGCAGAC	Sigma-Aldrich	N/A
NimC1 (F) ATCGAGTGGTCAACTGGTGTG *(R)* GTCAGGAATCCGTACCTCAGC	Sigma-Aldrich	N/A
Upd2 (F) ACAACCTGCGACTCTTCTCC *(R)* CAGATTGCCGTACTCCAGGG	Sigma-Aldrich	N/A
Upd3 (F) TCTGGACTGGGAGAACACCT *(R)* CTCACTGTGGCCAGCTTGT	Sigma-Aldrich	N/A
Trol (F) TACTCCTGCGTTGCCGAAAA *(R)* AATCTTTACACTCGGCCGCT	Sigma-Aldrich	N/A
Viking (F) TTCTGGGCGTCGTTTATCTGT *(R)* CTTTGCAGTCGCATAGCGTT	Sigma-Aldrich	N/A
Col4alpha1 (F) AGGCTTAAGTGCATAGGGCAT *(R)* TTGTAGTGTTTCACGGAGTCCT	Sigma-Aldrich	N/A
Software and algorithms		
Fiji	N/A	RRID:SCR_002285; https://fiji.sc/
IMARIS	Oxford Instruments	RRID:SCR_007370
CytExpert software	Beckman Coulter	RRID:SCR_017217
BD FACSDiva Software	BD (Becton Dickinson)	RRID:SCR_001456
GraphPad Prism v10.1	GraphPad Software Inc.	RRID:SCR_002798; https://www.graphpad.com/scientific-software/prism/

(*Continued on next page*)

Continued

REAGENT or RESOURCE	SOURCE	IDENTIFIER
FlowJo™ v10.10.0	FlowJo Inc.	RRID:SCR_008520; https://www.flowjo.com/solutions/flowjo/downloads
Biorender.com	Biorender	RRID:SCR_018361; https://www.biorender.com
Adobe Illustrator v27.9.1	Adobe	RRID:SCR_010279; https://www.adobe.com/products/illustrator.html
Leica Application Suite X	Leica	RRID: SCR_013673; https://www.leica-microsystems.com/products/microscope-software/details/product/leica-las-x-ls/

RESOURCE AVAILABILITY

Lead contact

Further information and requests for reagents should be directed to and will be fulfilled by corresponding authors E. Gomez Perdiguero (elisa.gomez-perdiguero@pasteur.fr) and A. Giangrande (angela@igbmc.fr). The lead contact is A. Giangrande.

Materials availability

This study did not generate new unique reagents.

Data and code availability

- Data reported in this paper will be shared by the lead contact upon request.
- This paper does not report original codes.
- Any additional information required to reanalyze the data reported in this paper is available from the lead contact upon request.

EXPERIMENTAL MODEL AND STUDY PARTICIPANT DETAILS

Fly lines

All flies were raised on standard media at 25°C. The following strains were used: w^{1118}(reference line), *HmlΔGal4, UAS-2XEGFP* (BDSC #30140), *HmlΔGal4* (BDSC #30139), *UAS-hid* (BDSC #65403), *stg* RNAi (BDSC 36094), *eater RNAi* (BDSC #25863), *trol RNAi* (BDSC 29440), *vkg RNAi* (BDSC 50895), *UAS-trol* (BDSC 65273), *UbiGal4* (BDSC #32551), *domeMeso-EBFP2* (gift from Jiwon Shim[70]). Optimized conditions were used to obtain stage-synchronized progeny. Adult flies were let lay on apple juice agar plates for 3 h at 25°C. The plates were transferred at 25°C or 29°C according to the experimental set up. L1 larvae were selected 24 h after egg lay, transferred in batches of 100 larvae on fresh medium and raised at the desired temperature until the stage of the analysis. Unless otherwise specified, male larvae were used to avoid gender-related variability since males and females show different organs/body size and macrophage number.

Mouse lines

All mice used in this study have been previously described. Experimental procedures, housing and husbandry were in compliance with the regulatory guidelines of the Institut Pasteur Committee for Ethics and Animal Experimentation (CETEA, dap160091). Strains included $Cdh5^{CreERT2}$ transgenic (C57Bl6 background, MGI:3848982) and $Rosa26^{tdTomato}$ mice. Timed matings were performed and the date of vaginal plug was considered E0.5. Embryonic stage was validated using morphological landmarks. Genotyping procedures are available upon request. To deplete macrophages, we used the selective CSF1R-inhibitor PLX5622. Control and PLX5622 (1200 ppm formulated in AIN-76A standard chow, Research Diets, Inc.) chows were kindly provided by Plexxikon Inc (Berkeley, CA) and administered to pregnant dams.

METHOD DETAILS

Fly macrophage immunolabeling

Macrophages were collected upon bleeding larvae in cold PBS 1X added with N-Phenylthiourea (Sigma-Aldrich P7629) to avoid cell melanization. The amount was adjusted according to the stage in analysis: 10 wL3 larvae were bled in 100 μl, 20 midL2 larvae were bled in 50 μl. Cells were let decant on the slide for 20 min at room temperature (RT) or cytospinned at 500 rpm for 3 min for lamellocyte immunolabeling due to the poor adhesion of lamellocytes to the slide by decantation. The cells were then fixed in 4% paraformaldehyde (PFA)/PBS 1X for 10 min, washed three times with PTX (0.3% Triton X-100 in PBS 1X) for 10 min, incubated 1 h in PTXN

(NGS 5% in PTX, Vector Laboratories), incubated ON at 4°C in primary antibodies diluted in PTXN. Cells were then washed with PTX for 10 min, incubated 1 h in secondary antibodies diluted in PTXN, incubated 1 h with DAPI (1:5000, Sigma-Aldrich), washed with PTX and then mounted with Vectashield mounting medium. The following primary antibodies were used: chicken anti-GFP (1:500, abcam ab13970), rabbit anti-Peroxidasin (1:2000, gift from J. Shim[93]), mouse anti-Hemese (1:50, gift from I. Ando[44]), mouse anti-PH3 (1:1000, Millipore 3H10), rabbit ati-Dcp1 (1:200, Cell signaling 9578), mouse anti-Atilla and mouse anti-L4 (1:50, gift from I. Ando[94]). The donkey anti-chicken FITC (Jackson ImmunoResearch # 703 095 155) and goat anti-mouse Alexa Fluor 647 (Jackson ImmunoResearch # 115 605 166), donkey anti-rabbit Cy3 (Jackson ImmunoResearch # 711-165-152) secondary antibodies were used at 1:400. For each marker, at least two independent experiments were performed.

Lymph gland immunolabeling

Lymph glands were dissected in PBS 1X, fixed in 4% PFA/PBS 1X for 30 min, washed three times with PTX for 10 min, incubated 1 h in PTXN, incubated ON at 4°C in primary antibodies diluted in PTXN. After 3 washes with PTX of 10 min each, lymph glands were incubated 20 min in PTXN, incubated 2 h in secondary antibodies diluted in PTXN, incubated 30 min with DAPI, washed twice with PTX, then transferred in PBS 1X and mounted with Vectashield mounting medium. The following primary antibodies were used in addition to those previously mentioned: rabbit anti trol (1:1000, gift from A. González Reyes[95]), rabbit anti Cg25c (1:500, gift from S. Noselli[96]), mouse anti-Antp (1:50, DSHB 4C3, DSHB 8C11), Rat anti-E-Cadherin (1:50, DSHB DCAD2), mouse anti-βPS integrin (1:50, DSHB CF.6G11), mouse anti-Wg (1:5, DSHB 4D4). See above for secondary antibodies.

Image acquisition on fly macrophages and lymph glands

Images were acquired using a Leica SP8 inverted-based confocal microscope equipped with 20, 40 and 63X objectives. A647/Cy5 was excited at 633 nm and emission signal was collected with 650-700 filters. GFP/FITC was excited at 488 nm and the emission signal was collected with 500-550 filters. RFP/Cy3 was excited at 561 nm and the emission signal was collected with 570-620 filters. Z-series images were acquired using a Z-step size between 0.5 and 2μm and applying identical settings for control and experimental genotypes. Confocal images were analyzed with Fiji software (RRID:SCR_002285).[97]

Transmission electron microscopy

Samples for transmission electron microscopy were prepared according to published protocols.[28] Briefly, early-midL2 larvae (~45 h after egg laying) raised at 29°C were dissected in 4% PFA/PBS 1X and incubated in a fixative solution of 3.2% EM grade PFA and 3.125% Glutaraldehyde at 4°C for at least 1 day. Post-fixation was carried out in 1% osmium tetroxide. Tissue was dehydrated through acetone series at 4°C, embedded with a graded series of epon:acetone mixtures at room temperature in flexible plastic mold and finally polymerized at 60 °C for 48 h. Ultra-thin serial sections of 70 nm were picked up on grids, contrasted with uranyl acetate and lead citrate and examined using a CM12 TEM electron microscope 100Kv (FEI) equipped with a CCD ORIUS 1000 Gatan Camera.

RNA extraction and RT-qPCR on fly macrophages and larvae

To assess the expression levels of genes of interest in macrophages, at least 30 earlyL2 (~48 h after egg laying) larvae from both sexes were bled in 100 μl of cold PBS 1X added with N-Phenylthiourea. RNA extraction was performed as follows. 1 ml of TRI-reagent (Molecular Research Center) was added to the collected macrophages, and the samples were left at RT for 5 min to ensure complete dissociation. 0.2 ml of chloroform was added to each sample followed by centrifugation at 12,000 g for 15 min at 4°C. The upper aqueous phase containing the RNA was collected and transferred to a fresh autoclaved tube. 0.5 ml of 2-propanol was added, and the samples were incubated for 10 min at RT. The RNA was precipitated by centrifugation, washed with 1 ml of 75% ethanol, precipitated again, and air-dried. 20 μl of RNase-free water was used to resuspend the pellet and the samples were incubation at 55°C for 15 min to facilitate the resuspension. The extracted RNA was then treated with DNase I recombinant RNase free (Roche) and the reverse transcription was done using the Super-Script IV (Invitrogen) with random primers. The cycle program used for the reverse transcription is 65°C for 10 minutes, 55°C for 20 minutes, 80°C for 10 minutes. The qPCR was performed using SYBR Green I Master (Roche). Actin5C (Act5C) and Ribosomal protein 49 (Rp49) were used to normalize the data.

To assess the expression levels of the ECM components *trol*, *vkg* and *Col4alpha1* upon ubiquitous induction of *trol RNAi*, total RNA from 4 control or *trol RNAi* wandering L3 larvae was extracted and treated as above described.

4OHT Preparation and Injection

4-hydroxytamoxifen (4OHT) (Sigma, H7904-25MG) was dissolved in equal parts of ethanol and Kolliphor EL (Sigma C5135-500G) by sonication. 10mg/mL stocks of progesterone (P3972-5G) were prepared by resuspending in ethanol and sunflower oil (Sigma S5007-250ML). For pulse-labeling, females were weighed on day 7 or 10 and 37.5μg/g (body weight) 4OHT were co-injected with 18.75μg/g (body weight) progesterone to reduce the risk of abortion.

Flow Cytometry

Pregnant mice were killed by cervical dislocation and embryos were dissected in cold PBS. Fetal peripheral blood was collected in 2mM EDTA by severing the vitelline and umbilical vessels after removing the placenta and extraembryonic membranes. Organs were enzymatically dissociated in digestion buffer composed of PBS with 1mg/mL collagenase D (Sigma 11088882001), 100 U/mL DNaseI

(DN25-100mg) and 3% Fetal Bovine Serum. Cells were passed through 100μm strainers by mashing with the piston of a 2mL syringe and then collected in cold filtered FACS Buffer (0.5% BSA and 2mM EDTA in PBS). Cells were then pelleted by centrifugation at 320*g* for 7 minutes. Blocking was performed with 5% FBS and 1:20 Mouse IgG (Interchim 015-000-003) or in 1:50 Fc-block (anti-CD16/32) in FACS Buffer followed by 30 minutes of antibody staining. Cells were washed and incubated with fluorescently-conjugated streptavidin for 20 minutes. For experiments with adult mice, blood was collected by retro-orbital bleeding. After sacrificing mice by cervical dislocation perfusion was performed by gentle intracardiac injection of 10 ml prewarmed (37°C) PBS. Adult tissues were minced with scissors before enzymatical digestion in digestion buffer composed of PBS with 1mg/mL collagenase D (Sigma 11088882001), 100 U/mL DNaseI (DN25-100mg), 2.4mg Dispase II (Invitrogen 17105-041) and 3% Fetal Bovine Serum. For livers, hepatocyte removal was performed by centrifugation of the whole liver single cell suspension at 50*g* for 3 minutes. For earskin, epidermal sheets were first separated from the dermis after incubation for 1h at 37°C in 2.4 mg/ml of Dispase II in PBS and the epidermis was further digested for 30 min in PBS containing 1 mg/ml collagenase D, 100 U/ml DNase I, 2.4 mg/ml of Dispase II and 3% FBS at 37°C. Bone marrow was flushed from the femur and tibia using a 25G needle. For red blood cell lysis, cells were resuspended in 1 ml of Red blood cell lysis buffer (155 mM NH_4Cl, 10 mM $NaHCO_3$, and 0.1 mM EDTA). The reaction was terminated after 5 min by adding 3 ml of FACS buffer. Lysis was performed once for adult livers and bone marrows and twice for adult blood samples. Stained cells were passed on the Cytoflex LX (Beckman Coulter). Results were analyzed and plots generated using FlowJo.

RNA extraction and quantitative qPCR on mouse fetal liver

Fetal livers were dissected in ice-cold PBS and directly transferred to RNAprotect (Qiagen, 76104) for short term-storage. After transfer of 10mg of fetal liver tissue into RLT buffer (RNeasy Plus Mini Kit, Qiagen, 74134) with 1% beta-Mercaptoethanol, livers were lysed and homogenized by bead-milling with a 5 mm stainless steel bead (Qiagen, 69989) in the TissueLyserII (Qiagen) twice for 2 min at 30 Hz. Total RNA was extracted from whole tissue lysate using the RNeasy Plus Mini Kit (Qiagen, 74134), using 50 % ethanol in step 5. cDNA was reverse transcribed using PrimeScript™ RT Reagent Kit (Perfect Real Time) (Takara, RR037A) and following manufacturer's instructions. Taqman assays (Mouse Immune array- Applied BiosystemsTM, 4418724 or customized mouse Extracellular Matrix and Adhesion molecules plates) were performed on a Quantstudio 3 thermocycler (Applied Biosystems, 50 °C 2 min, 95 °C 20 sec, 40 cycles : 95 °C 3 sec and 60 °C 30 sec, 60 °C 30 sec) using 20 ng of cDNA in 1x TaqMan™ Fast Advanced Master Mix (Applied Biosystems™, 12634225) per well. Gene expression was normalized to *gapdh* or *hprt1* and relative expression was calculated using the 2^{-and} method.

Fetal liver immunolabeling

Dissected fetal livers were fixed in 5 % Formalin solution containing 2 % formaldehyde (Sigma) in PBS at 4 °C overnight, washed 3 times in PBS, immersed in 30% sucrose overnight, cryoembedded in OCT (Tissue-Tek) and stored at -80 °C. 12μm thin sections were cut on a Leica Cryostat at -25 °C. Sections were washed in PBS for 5 min, permeabilized in PBS-Triton 0.5% (PBS-T) for 5 min, washed in PBS for 5 min and finally blocked in 5 % normal goat serum in 0.1 % PBS-T for 1 hour. Fetal liver sections were stained with primary antibodies in blocking solution for 1 hour (rabbit anti-mouse Collagen IV 1:200 (Biorad, 2150-1470)), washed 3 times in 0.1 % PBS-T for each 5 min, stained with secondary antibodies (goat anti-rabbit AF555 1:500 (Invitrogen, A-21429)) and washed 3 times in 0.1 % PBS-T. Permeabilization, blocking and staining were all performed at room temperature. Stained sections were covered with ProLong™ Gold Antifade Mounting (Invitrogen, P36930). Sections were imaged as z-stacks of 8 μm depth (9 planes with a distance of 1 μm) in tilescans using an inverted Leica SP8 confocal microscope with a HC PL APO 20x/0,75 CS2 objective (Leica, 11506517) and the LasX software. AF555 was excited at 552 nm and the emission signal was collected with a HyD detector set at 562-600nm. Final image processing (flipping of images and adding of scale bars) was performed in Fiji.[97]

Fetal Liver TUNEL Assay

Fresh 100μm thick fetal liver (FL) sections were prepared as mentioned elsewhere.[98] Sections were permeabilized and blocked in 10% Normal Goat Serum in PBS-Triton 0.5% (PBS-T) for 2 hours at room temperature, incubated with rat anti-mouse CD68 (1:100) in bocking solution overnight at 4C and finally washed 3x 20 min in 0.1% PBS-T. Secondary staining was performed by incubation with goat anti-rat AF555 (1:500) in 0.1 % PBS-T for 2h at room temperature in the dark. FL sections were washed 3x 20 min in 0.1% PBS-T. Thick sections were incubated in 200μL of TUNEL reaction mix (Roche, Cat. No. 12156792910) for 1h at 37°C, washed 2x15 min in PBS and cleared in RapiClear (1.52) overnight. Sections were mounted in RapiClear and imaged with a *Leica SP8* confocal microscope with a 63x objective (immersion oil) and a 40μm deep z-stack was acquired. Maximum projections were generated in *Fiji*[97] and CD68 AF555 exposure was enhanced for better visibility of the signal.

Proliferation assay

To assay proliferation, single cell suspensions were stained for cell surface proteins as described above. Following the staining, cells were fixed and permeabilized in 4% Fixation/Permeabilization buffer (BD, Cat. No. 554714) for 20 minutes on ice, washed, then stained with intracellular markers (Ki67, 1:50; SYTOX green, 1:1000) in BD Perm/Wash™ for 1 hour on ice, washed in BD Perm/Wash™ and finally resuspended in FACS buffer. Stained cells were passed on the Cytoflex LX and SYTOX green was recorded in linear.

Single cell liquid culture

Single cell suspensions from fetal livers and adult bone marrows were prepared and blocked as described above. Lineage positive cells (Ter119$^+$ CD19$^+$ CD3e$^+$ CD4$^+$ CD8$^+$ NK1.1$^+$ F4/80$^+$ Gr1$^+$) were depleted using magnetic anti-biotin Microbeads (1:5) (Miltenyi Biotec 130-090-485) and MS columns (Miltenyi Biotec 130-042-201). CMPs (Live (SYTOX green, Thermo Fisher), Lin$^-$ Kit$^+$ Sca-1$^-$ CD127$^-$ CD34$^+$ CD16/32^{int}) were sorted using a FACSAria III (Diva software) and cloned into flat-bottom 96-well plates (UpcellNUNC) containing pre-warmed and equilibrated differentiation medium (0.1% β-mercaptoethanol, 1X Penicillin/Streptomycin, 10% FBS, 1:125 SCF, 5ng/μL GM-CSF, 5ng/μL M-CSF, 2ng/μL EPO and 5ng/μL TPO in Opti-MEM with Glutamax). SCF was supplied from myeloma cell line supernatant. Cells were grown at 37 °C with 5% CO_2 for 7 days. Colony analysis was performed first by manually scoring wells for the presence of colonies and identification of Megakaryocytes (Mk), centrifugating plates at 320*g* for 7 minutes at 4 °C and staining each colony for 1 hour at 4 °C with 40 μL of antibody mix containing 1:400 Fc-block (anti-CD16/32) and 1:400 anti-CD45, -CD11b, -Ly6G, -Ly6C, -IL33Ra(ST2), -Kit, -Ter119, -CD41. Stained colonies were collected for flow cytometry analysis by scratching. Cells were identified by the following markers: Macrophages: CD45$^+$ CD11b$^+$, F4/80$^+$, Monocytes: Neutrophils: CD45$^+$, CD11b$^+$, Ly6G$^+$, Mast cells: CD45$^+$ Kit$^+$ IL33Ra (ST2)$^+$, Red blood cells: CD45$^-$ Ter119$^+$, Megakaryocytes: CD41$^+$.

QUANTIFICATION AND STATISTICAL ANALYSIS

Quantification

Fly lymph gland's volume, cellularity (number of DAPI$^+$ nuclei) as well as number of PH3$^+$, Hml$^+$, Antp$^+$ cells were measured with IMARIS software (RRID:SCR_007370) based on confocal images. For fly macrophage counting, 10 larvae were bled in 100 μl (wL3) or 50 μl (L2) of cold PBS 1X added with few crystals of N-Phenylthiourea. The bleeding was performed by peeling the dorsal and ventral cuticle of the larva in order to release macrophages. Cells were then counted in brightfield with a hemocytometer (volume of counting: 1 μl) and the following formula was used to estimate the number of macrophages/larva: (# of macrophages counted in 1 μl) x (bleeding volume)/10. For flow cytometry, the following formula was used to quantify cells: (# of cells acquired) x (volume of resuspended cells after staining and washing/volume of cells acquired) x (volume of cell suspension in blocking buffer prior to staining/volume of cells plated for staining) and divided by the weight of analyzed adult tissue where applicable. Flow data was analyzed by FlowJo and plots were generated using Graphpad Prism.

Statistical analysis

Two tailed unpaired t-test was used to estimate p-values for fly macrophage number and gene expression level, lymph gland cellularity, volume and number of PH3$^+$, Hml$^+$, Antp$^+$ cells. Flow cytometry data was quantified in Graphpad Prism using Tukey multiple comparisons test for time course analysis, One-way ANOVA for comparisons of multiple different populations within one sample and Mann-Whitney test for pairwise comparisons The number of animals used in each experiment and other experimental details are indicated in the figure legends.